https://doi.org/10.1016/j.jclepro.2021.128716

An Interactive Tri-Level Multi-Energy Management Strategy for Heterogeneous Multi-Microgrids

Yingping Cao[a,b,c], Bin Zhou[a*], Siu Wing Or[b,c], Ka Wing Chan[b], Nian Liu[d], Kuan Zhang[a]

[a]*College of Electrical and Information Engineering, Hunan University, Changsha 410082, China*
[b]*Department of Electrical Engineering, The Hong Kong Polytechnic University, Hung Hom, Kowloon, Hong Kong*
[c]*Hong Kong Branch of National Rail Transit Electrification and Automation Engineering Technology Research Center, Hong Kong*
[d]*State Key Laboratory of Alternate Electrical Power System with Renewable Energy Sources, North China Electric Power University, Beijing 102206, China*

Abstract: This paper proposes a multi-level multi-energy management framework for the coordinated and interactive operation of heterogeneous multi-microgrids (MMGs) based on many-criteria optimality. With the proposed framework, the highly nonlinear and complex MMG multi-energy management (MMGMEM) problem is formulated into tri-level scheduling subproblems with multi-energy couplings and multi-level interactions, in which the multi-energy trading with energy networks and multi-energy couplings within MGs are optimized in the upper and middle level, and a middle level is added to correct scheduling decisions of the upper level for coordinating the MMG multi-energy sharing. Then, a multi-step matrix decomposition technique is developed to decompose the high dimensional multi-energy coupling matrix of MMGs into the sum of three linear and sparse submatrices for improving the computation efficiency and scalability. Furthermore, a many-criteria decision making (MCDM) model is proposed for the multi-energy sharing problem to achieve an optimum tradeoff in which all microgrids (MGs) can benefit from electricity-gas exchanges, and an evolutionary many-objective optimization based on hyperplane transformation algorithm is used to solve the MCDM problem. Simulation results verify that the proposed framework can achieve a cost saving for each MG (over 19%), and validate its scalability in solving large-scale MMGMEM problems.

Keywords: Multi-energy management, multi-level scheduling, many-criteria optimality, renewable energy, multi-microgrids.

Highlights

A tri-level interactive framework is proposed for the coordinated operation of MMGs.
An extended multi-energy coupling matrix with MMG interactions is formulated.
A multi-step matrix decomposition technique is used to reduce the problem complexity.
A many-criteria optimality model is proposed for the tradeoff of all MGs' benefits.
The utilization of renewables can be enhanced with the minimal total operation cost.

* Corresponding author at: College of Electrical and Information Engineering, Hunan University, Changsha 410082, China.
E-mail address: binzhou@hnu.edu.cn (Bin Zhou).

Nomenclature

Sets, Indices and Function

m	Index of MGs
f^{WT}/ f^{PV}	Power generation function of wind turbine (WT)/ photovoltaics
$\boldsymbol{I}_{m,1}$/$\boldsymbol{I}_{m,2}$/$\boldsymbol{I}_{m,3}$/ $\boldsymbol{I}_{m,4}$/$\boldsymbol{I}_{m,5}$	Sets of P2G/boiler/CHP/furnace/BESS/gas tank in MG m
$iter$	Index of iteration number of EMOHT

Parameters

$\eta^{\mathrm{CHP,H}}$/$\eta^{\mathrm{CHP,E}}$	Gas-to-thermal/gas-to-electric efficiency of CHP
η^{ch}, η^{dis}	Charging/discharging efficiency of BESS
η^{Boi}/η^{Fur}/η^{P2G}	Conversion efficiency of boiler/furnace/P2G
Q^{Gas}	Heat value of gas (MJ/m^3)
W_m^{WT}/G_m^{PV}	Input of wind speed/solar irradiation in MG m
$C_t^{\mathrm{buy,Gas}}$/ $C_t^{\mathrm{sell,Gas}}$	Purchase/sale price of gas at time slot t (\$/m^3)
$C_t^{\mathrm{buy,E}}$/$C_t^{\mathrm{sell,E}}$	Buying/selling price of electricity at time slot t (\$/kWh)
$C_{m,i}^{\mathrm{CHP}}$/$C_{m,i}^{\mathrm{Boi}}$/ $C_{m,i}^{\mathrm{Fur}}$	Unit start-up cost of the CHP/boiler/furnace i in MG m (\$)
T	The prediction horizon in rolling optimization
$V_{m,i}^{\mathrm{P2G,min}}$/ $V_{m,i}^{\mathrm{P2G,max}}$	The lower/upper bound of ith P2G output in MG m (m^3)
$P_{m,i}^{\mathrm{BESS,ch,max}}$/ $P_{m,i}^{\mathrm{BESS,dis,max}}$	Maximum charging/discharging power of BESS i in MG m (kW)
$E_{m,i}^{R}$/$V_{m,i}^{R}$	Rate capacity of BESS/gas storage tank i in MG m (kWh)
$V_{m,i}^{\mathrm{Tank,ch,max}}$	Maximum charging/ discharging rate of the gas storage tank i in MG m (m^3/h)
$V_{m,i}^{\mathrm{Tank,dis,max}}$	
$SOC_{m,i}^{\mathrm{Tank,min}}$/ $SOC_{m,i}^{\mathrm{Tank,max}}$	Minimum/maximum SOC value of gas storage tank i in MG m
$P_{m,i}^{\mathrm{CHP,min}}$/ $P_{m,i}^{\mathrm{CHP,max}}$	The allowed minimum/maximum output of CHP i in MG m (kW)
$Q_{m,i}^{\mathrm{Boi,min}}$/ $Q_{m,i}^{\mathrm{Boi,max}}$	The allowed minimum/maximum output of boiler i in MG m (kW)
$Q_{m,i}^{\mathrm{Fur,min}}$/ $Q_{m,i}^{\mathrm{Fur,max}}$	The allowed minimum/maximum output of furnace i in MG m (kW)
$C_{m,i}^{\mathrm{Increase,P}}$/ $C_{m,i}^{\mathrm{Increase,G}}$	Unit cost of energy device i for increasing energy generation in MG m
$P^{\mathrm{CCDG,min}}$/ $P^{\mathrm{CCDG,max}}$	The allowed minimum/maximum output of CCDG (kW)
$R^{\mathrm{CCDG,down}}$/ $R^{\mathrm{CCDG,up}}$	Lower/upper bound of the ramp rate of CCDG (kW/h)
$E^{\mathrm{CBESS,R}}$	The rated capacity of CBESS (kWh)
$SOC_{\min}$/ $SOC_{\max}$	Lower/Upper bound of SOC for CBESS
$\Delta P_{m,i,t}^{\max}$/ $\Delta V_{m,i,t}^{\max}$	Maximum value of increasable capacity of the energy storage/conversion device i in MG m
$P_{\max}^{\mathrm{line}}$	Maximum capacity of electrical lines (kW)
$V_{\max}^{\mathrm{pipeline}}$	Maximum capacity of gas pipelines (m^3)
M	the total number of MGs

Variables

P_m^{BESS}/ V_m^{Tank}	Output of BESS (kW)/gas tank (m^3) in MG m
v_m^{E}/v_m^{H}/v_m^{G}	Dispatch factor of input energy resources to electrical/thermal/ gas load in MG m
v_m^{CHP}/v_m^{Boi}/ v_m^{Fur}/v_m^{P2G}	Dispatch factor of input energy resources to CHP/boiler/furnace/ P2G in MG m
$V_{m,t}^{\mathrm{short,Gas}}$/ $V_{m,t}^{\mathrm{sur,Gas}}$	Amount of shortage/surplus gas at time slot t in the MG m (m^3)
$P_{m,t}^{\mathrm{short,E}}$/ $P_{m,t}^{\mathrm{sur,E}}$	Amount of shortage/surplus electricity at time slot t in the MG m (kW)
$Q_{m,t}^{\mathrm{Boi}}$	Output of the electric boiler in the MG m (kW)
$Q_{m,t}^{\mathrm{Fur}}$	Output of the furnace in the MG m (kW)
$V_{m,t}^{\mathrm{P2G}}$	Output of the P2G system in the MG m (m^3)
$P_{m,t}^{\mathrm{CHP}}$	Output of the CHP in the MG m (kW)
μ_t/v_t/ω_t,/τ_t	Start-up indicators for energy converters
$P_{m,i,t}^{\mathrm{BESS,dis}}$/ $P_{m,i,t}^{\mathrm{BESS,ch}}$	Charging/discharging power of BESS i at time slot t in the MG m (kW)
$SOC_{m,i,t}^{\mathrm{BESS}}$/ $SOC_{m,i,t}^{\mathrm{Tank}}$	SOC of the BESS/the gas storage tank
$P_{m,i,t-\Delta t}^{\mathrm{BESS,ch}}$/ $P_{m,i,t-\Delta t}^{\mathrm{BESS,dis}}$	Charging/discharging power of BESS i at time slot t-Δt in the MG m (kW)
$\delta_{m,i,t}$/ $\varphi_{m,i,t}$	Binary variables that are used to indicate the state of BESS charging/discharging
$V_{m,i,t-\Delta t}^{\mathrm{Tank,ch}}$/ $V_{m,i,t-\Delta t}^{\mathrm{Tank,dis}}$	Rate of gas charging/discharging for the gas storage tank (m^3/h)
$\psi_{m,i,t}$/$\phi_{m,i,t}$	Binary variable representing the state of tank charging/ discharging
$P_{m,t}^{\mathrm{CBESS,dis}}$/ $P_{m,t}^{\mathrm{CBESS,ch}}$	Discharging/charging power of the CBESS at time slot t in the MG m (kW)
$V_t^{\mathrm{buy,Gas}}$/ $P_t^{\mathrm{buy,E}}$	Total amount of gas (m^3)/ electricity (kW) purchased from energy networks
$V_t^{\mathrm{sell,Gas}}$/ $P_t^{\mathrm{sell,E}}$	Total amount of gas (m^3)/electricity (kW) that is sold to the energy networks
$\Delta P_{m,i,t}$/ $\Delta V_{m,i,t}$	Increased energy output of energy devices i at time slot t in MG m
$V_{m,t}^{\mathrm{sell,Gas}}$/ $P_{m,t}^{\mathrm{sell,E}}$	The amount of gas/electricity sold to energy networks for MG m at time slot t
$V_{m,t}^{\mathrm{buy,Gas}}$/ $P_{m,t}^{\mathrm{buy,E}}$	Gas/electricity purchased from external energy networks
P_t^{CCDG}	Outputs of CCDG (kW)
$f_{m,\min}$	Minimum value of objective of mth MG
$iter_{\max}$	Maximum iteration number of EMOHT

Vectors and Matrix

$\boldsymbol{L}$	Column vector of the input energy
$\boldsymbol{S}$	Column vector of the output energy
$\boldsymbol{M}$	Coupling matrix
$\boldsymbol{S}_{\mathrm{sys}}$	System dispatchable capacities
$\boldsymbol{I}$	Identity matrix

1 Introduction

Nowadays, microgrids (MGs) have been increasingly recognized as an important and effective way to facilitate the integration of various distributed renewables, local loads and energy storage systems (Dey et al., 2021). It is reported by the United States Department of Energy that up to 13000 MW of loads can be supplied by MGs until 2020, with a growth rate of 15.8% over the last few years (Karimi and Jadid, 2020). The increasing penetration of solar and wind energy at the consumption premises can provide MGs with an environmentally friendly, free and abundant share of renewable energy supply. Due to the inherent intermittency and undispatchability of renewable energy resources, the entire output of renewable generators in an individual MG may exceed its load demand during low load periods, resulting in the curtailment of wind and solar generation. On the other hand, other MGs with high demand have to purchase electricity from energy networks at a high price to fulfill their load demand, leading to expensive operating costs (Yang et al., 2019). In general, multiple heterogeneous MGs can be connected to form a multi-microgrid (MMG) system. Compared with the individual MG, the MMG system is recognized as an effective measure to promote the utilization of renewable energy and minimize MGs' operation costs by sharing the surplus renewables among MGs (Daneshvar et al., 2020).

In a traditional MMG system, various loads are generally supplied by electricity generated with steam turbines using fossil fuels, wind turbines, and solar photovoltaic (PV) systems. With the rapid growth of electrical and thermal demands, the natural gas-fired combined heat and power (CHP) units, and power-to-gas (P2G) systems have been extensively employed to provide electricity, thermal energy, and combustible gas for multi-energy MGs (Zeng et al., 2021). Consequently, the electrical MMG gradually transforms towards a MMG system with multi-carrier energy forms, and multi-energy couplings and interactions among various types, qualities, and quantities of energy carriers have strengthened the complexity of the energy management problem of MMGs (Xu et al., 2020). Recent advancements on power electronics, smart meters, and communication technologies have offered great potential for the interactive multi-energy management within MMGs (Arefifar et al., 2017). The energy management of MMGs is a challenging nonlinear optimization problem due to multi-energy couplings within MGs, multi-energy exchanges among MGs, and multi-energy trading with external energy networks (Zhou et al., 2021). Furthermore, as heterogeneous MGs often exhibit different profit-seeking behaviors from the benefits of multi-energy sharing and trading, the multi-energy exchanges among MGs without coordination may cause competitive behaviors and thus degrade the system-wide performance. Therefore, a new generation of MMG multi-energy management (MMGMEM) strategy to coordinate the operations of heterogeneous MGs is becoming a pressing need for the overall economic efficiency enhancement.

So far, the energy management of electrical MMGs has been investigated extensively from the perspectives of economy, security and environment (Zhou et al., 2020a). To name a few, Bui et al. (2016) proposed a multi-agent based energy management strategy for MMGs to obtain a reduction of the operation cost and ensure the reliability of electricity supply. In our previous work (Zhou et al., 2020b), a bilevel house-aggregator-grid framework based on many-criteria optimality was developed to coordinate the multi-house demand response and mitigate the transformer damages during peak-load hours. Aghdam et al. (2020) employed a chance-constrained programming based approach for the day-ahead energy management of MMGs to reduce emissions of greenhouse gases. Khalili et al. (2021) proposed an original optimization framework for the risk-based scheduling of MGs to maximize the MG's profit and minimize the risk in profit from the demand response program, while the uncertainty of renewable energy is considered. Nonetheless, other energy forms were neglected. To effectively manage different energy forms in MMGs, recently, some efforts have been devoted to developing MMG multi-energy management frameworks, models, and strategies (Zhou et al., 2021). In (Shams et al., 2019), the optimal scheduling of thermal energy and electricity in MMGs was formulated as a stochastic model. In (Yang at al., 2021), a transactive energy mechanism-based energy sharing strategy was proposed for the economic operation of multi-energy MMGs.

With the increasing number of interconnected MMGs, the large-scale MMG multi-energy management problem was formulated as a hierarchical optimization model to reduce the computation complexity. For instance, in (Yazdani-Damavandi et al., 2018), a bi-level multi-energy management strategy was proposed to maximize profits of multi-energy players and to optimally determine the amount of multi-energy exchange between players and MGs. A hierarchical energy management system was applied in (Bui et al., 2019) for the optimal multi-energy sharing among building MGs to minimize the system operation cost. Wang et al. (2018) presented a two-stage energy management strategy for networked MMGs, where the first stage minimized the MMG operation cost, and the second stage minimized the imbalance cost due to the deviations between the real-time and day-ahead markets. In (Yuan et al., 2020), a bi-level optimization framework was developed, in which the upper level optimality determined the electrical price for increasing the profit of suppliers, and the lower level optimized the energy scheduling to maximize the MMG welfare. However, for all these works on the hierarchical framework, the upper level makes optimized decisions from the perspective of global MMGs without considering the optimization objective of each MG at the lower level, and thus the scheduling decisions from the upper level may not be optimum for each MG.

In most cases, the multi-energy MG can be formed as an energy hub to map input energy sources to multi-energy demands (Moeini-Aghtaie et al., 2014), and a coupling matrix is usually formulated to model the multi-energy conversion and storage (Liu et al., 2019). Based on the energy hub, operation state

calculations (Xu et al., 2020), power flow optimizations (Shao et al., 2017), and investment analyses (Xuan et al., 2021) for MGs were investigated. In the matrix modeling, a comprehensive input-output matrix approach was presented in (Chicco and Mancarella, 2009) to model a small-scale tri-generation system, and a standardized modeling method based on graph theory was developed in (Liu et al., 2019) to reduce the difficulty of formulating the coupling matrix of a complex energy hub model. In (Wang et al., 2019), a matric modeling method was proposed to cast characteristics of energy converters and topologies of the multi-energy system into matrix form automatically. Besides, various matrix calculation methods, including the path searching method (Chicco and Mancarella, 2009) and the variable substitution method (Shao et al., 2017), have been used to address the nonlinearity of the coupling matrix or solve it. However, all mentioned methods are well applied in a single MG, and the multi-energy coupling matrix for describing multi-energy interactions among MMGs is not involved yet. Moreover, the multi-energy coupling matrix for MMGs is a high dimensional and strongly nonlinear matrix, which is hard to be solved with existing methods. Therefore, an advanced matrix decomposition technique is required to reduce its computational complexities in the optimum iterative procedure.

The MMG multi-energy management problem involves the coordinated operation of multiple MGs with various multi-energy converters and storages. Various multi-objective optimization models for MGs have been developed for efficient renewable energy utilization, operation cost reduction, and reliability improvement (Jafari et al., 2020a). For example, a multi-objective energy management model for MMGs was presented in (Tan and Chen, 2020) to minimize the operating costs, transmission losses, and carbon emissions of MMGs. A bi-level multi-objective optimization model for MGs was formulated in (Dissanayake and Ekneligoda, 2020) to reduce power losses, improve voltage profiles and minimize investment costs. In (Huang et al., 2019), a multi-objective optimization model for hybrid energy systems was proposed to reduce system costs, losses of power supply and potential energy wastes. Nevertheless, these models can't guarantee the optimum coordination for competitive and interactive behaviors among MMGs considering multi-energy couplings. Furthermore, different utility functions, including the cost function of energy consumptions (Li et al, 2018), the cost function of generator and storage investment, the cost function of pollutant treatment (Lu et al., 2018), have been presented for MMGs, while satisfying the supply-demand balance target. In (Jafari et al., 2020b), a novel techno-economical objective function was proposed for guaranteeing the profits of all individual MGs, reducing the energy that is not supplied, and improving the reliability of MMGs. Nevertheless, existing investigations mainly focus on maximizing the economic benefits of MMGs or individual MG, and few works have attempted to coordinate the operation of MMGs for the best tradeoff of their benefits from multi-energy sharing.

To sum up, although different aspects of energy management for MMGs have been investigated in previous works, none of the aforementioned investigations modeled the multi-energy coupling matrix of MMGs to describe multi-energy interactions among MMGs, and an advanced matrix decomposition technique for reducing its computational complexities was not involved. Furthermore, the coordinated and interactive operation of MMGs for achieving an optimum trade-off of MMG benefits from the multi-energy sharing was also neglected. Hence, this paper endeavors to fill these gaps by proposing an interactive tri-level multi-energy management strategy to coordinate the operation of heterogeneous MGs based on many-criteria optimality. With the proposed strategy, the optimum multi-energy management problem of MMGs can be decomposed into multi-energy trading with energy networks in the upper level, multi-energy sharing among MGs in the middle level, and the multi-energy coupling within MGs in the lower level, and thus the interactions of multiple levels can facilitate the coordinated operation of MMGs and the local integration of renewable energy. The key contributions of this paper are summarized as follows:

1. A tri-level interactive multi-energy management framework is proposed for optimum synergies of MMGs to minimize the overall system operation cost and enhance the utilization of renewable energy. The upper level minimizes the global MMG operation cost, and the lower level aims to optimize the multi-energy conversion and storage pathways within each MG for reducing its operation cost. Compared with previous hierarchical frameworks, a middle level is added to further correct the multi-energy scheduling decision from the upper level for ensuring the impartial allocation of the total sharing amount of multi-energy sources among MMGs.

2. A MMG multi-energy coupling matrix is developed to model and exploit inherent multi-energy couplings within individual MGs and external electricity-gas interactions among MMGs. Furthermore, a multi-step matrix decomposition technique is proposed to decompose the high dimensional and nonlinear coupling matrix of MMGs into the sum of three linear and sparse submatrices, and the proposed technique can significantly improve the efficiency of computational iterations and exhibit high flexibility for the scalability with MMG interconnections.

3. The multi-energy sharing process among multiple heterogeneous MGs is formulated as a many-criteria optimality model to achieve an optimum tradeoff for ensuring the coordination and equilibrium of all MGs' benefits. Then, an evolutionary many-objective optimization based on hyperplane transformation (EMOHT) algorithm is presented to solve the many-criteria decision making (MCDM) problem of multi-energy sharing, and the flexibility of multi-energy conversion and interaction can be utilized to determine the optimum amount of electricity-gas exchanges among MMGs for the reduced operation cost of each MG.

The rest of this paper is organized as follows: The problem formulation is presented in Section 2; The

proposed tri-level multi-energy management strategy for MMGs is formulated in Section 3; The performance of the proposed model is demonstrated through simulation studies in Section 4; Finally, conclusions are drawn in Section 5.

2 Problem Formulation

2.1 Configuration of multi-energy MMGs

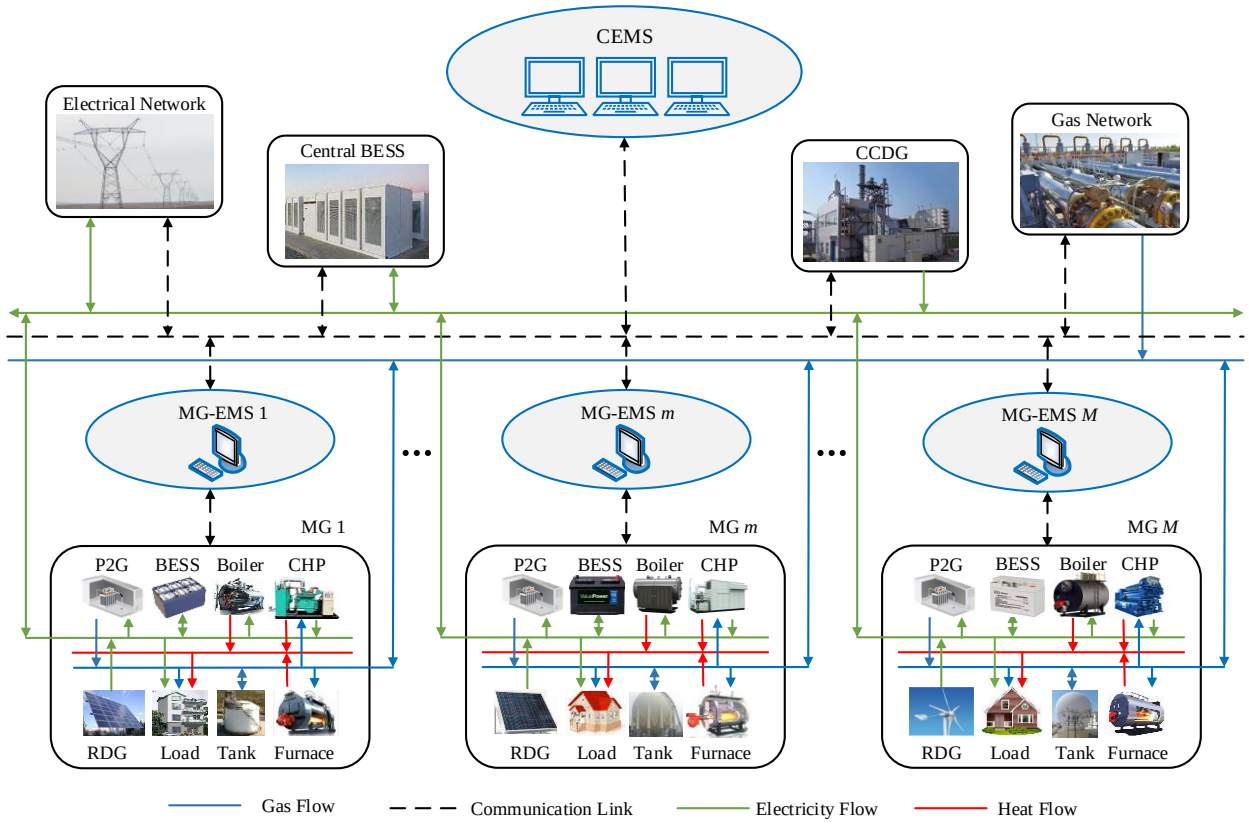

Fig. 1 Multi-level framework for the coordinated MMGMEM.

This study investigates the optimum multi-energy management problem of a MMG system composed of multiple heterogeneous MGs. Each MG contains renewable distributed generators (RDGs), P2G systems, CHPs, battery energy storage systems (BESSs), and other various energy converters and storages. The MMG system devices are comprised of central BESSs (CBESS) and central controllable distributed generators (CCDG). The schematic diagram of the MMGMEM is shown in Fig.1. In each MG, energy resources derived from renewable energy and energy networks can be converted and conditioned by energy converters and storages to satisfy the multi-energy demands. Besides, the MG having surplus electricity and gas can directly trade with the energy networks or share with other MGs, while the MG with shortage energy can buy energy from energy networks or receive energy from other MGs. The communication and control for MMGs and each MG are performed by the central energy management system (CEMS) and the

MG-EMS, respectively, through the advanced metering infrastructure and optical fiber deployed at the participation premises (Bui et al., 2016). During the energy exchange process, competitive events appear among different MGs for deriving their profits.

2.2 Multi-energy interactions within MMGs

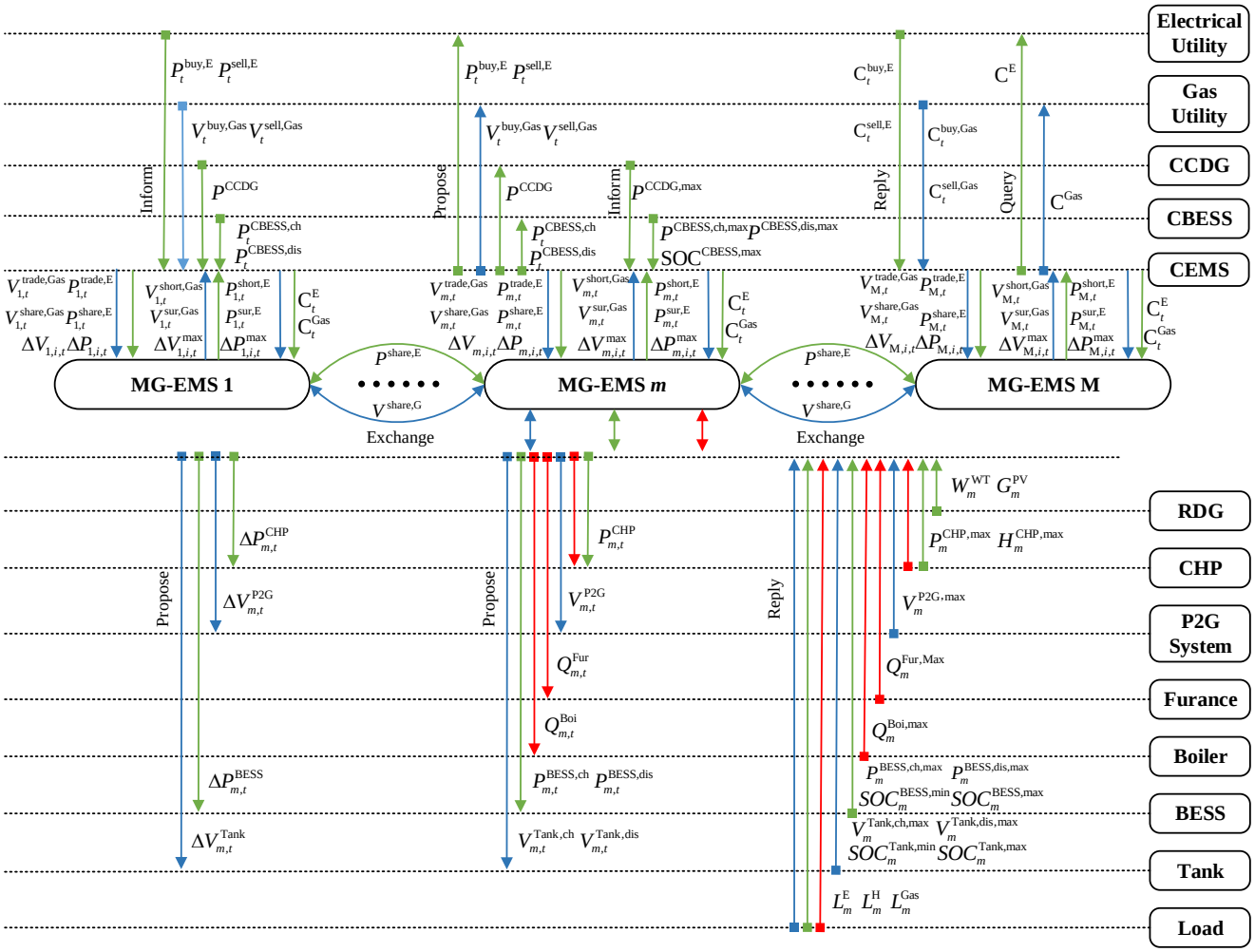

Fig. 2 Multi-energy interactions within MMGs.

The multi-energy interactions within the MMGs are described in Fig. 2. At the lower level, a message is sent by CEMS to the energy companies for querying about market prices, and companies send their buying and selling price signals to reply to queries of CEMS. These price signals are then destined to MG-EMSs. Based on the information received from their energy devices and CEMS, MG-EMS performs the local optimization to optimally schedule multi-energy conversion and storage devices for satisfying its load demand with minimal operation cost, and decides whether it participates in global optimization. Then, if MGs participate in global optimization, MGs with surplus energy will inform CEMS about their surplus and increasable energy, while other MGs with shortage energy make a purchase request to the CEMS. At the upper level, after receiving request signals from all MG-EMSs, CEMS will perform the global

optimization to determine outputs of system devices, amounts of energy traded with energy networks, and amounts of energy generation to be increased for each MG. At the middle level, CEMS will further correct the scheduling decisions from the upper level to coordinate the multi-energy sharing among MMGs, and then control signals about energy trading and sharing are delivered to each MG-EMS. For information privacy issues (Gansterer and Hartlm, 2018), in this process, each MG-EMS only shares the information in terms of the surplus/shortage amount of energy and the increasable energy with CEMS, while the sensitive private information of each MG, including operational parameters of energy devices, generation data of RDGs and multi-energy demands, is confined to the respective MG-EMS.

2.3 MMG multi-energy coupling matrix

To explicitly exhibit the multi-energy couplings within the MG, an energy hub model is developed to map the input energy sources to local multi-energy demands, while the conversions and storages of different energy carriers are modeled and characterized by a multi-energy coupling matrix $\boldsymbol{M}_{m,m}$, as shown in (1). Each element of the matrix is termed as a coupling factor to represent conversion efficiencies and connection topologies among energy converters and storages. Then, a MMG energy coupling matrix (2) is developed to model multi-energy couplings within MGs and multi-energy interactions among MMGs.

$$\underbrace{\begin{bmatrix} L_m^{\mathrm{E}} \\ L_m^{\mathrm{H}} \\ L_m^{\mathrm{Gas}} \end{bmatrix}}_{\boldsymbol{L}_m} = \underbrace{\begin{bmatrix} f^{\mathrm{WT}} v_m^{\mathrm{E}} & f^{\mathrm{PV}} v_m^{\mathrm{E}} & v_m^{\mathrm{E}} & Q^{\mathrm{Gas}} \eta^{\mathrm{CHP,E}} v_m^{\mathrm{CHP}} v_m^{\mathrm{E}} \\ f^{\mathrm{WT}} \eta^{\mathrm{Boi}} v_m^{\mathrm{Boi}} v_m^{\mathrm{H}} & f^{\mathrm{PV}} \eta^{\mathrm{Boi}} v_m^{\mathrm{Boi}} v_m^{\mathrm{H}} & \eta^{\mathrm{Boi}} v_m^{\mathrm{Boi}} v_m^{\mathrm{H}} & \begin{array}{l} Q^{\mathrm{Gas}} (\eta^{\mathrm{CHP,E}} v_m^{\mathrm{CHP}} v_m^{\mathrm{Boi}} \eta^{\mathrm{Boi}} + \\ \eta^{\mathrm{CHP,H}} v_m^{\mathrm{CHP}} + \eta^{\mathrm{Fur}} v_m^{\mathrm{Fur}}) v_m^{\mathrm{H}} \end{array} \\ f^{\mathrm{WT}} \eta^{\mathrm{P2G}} v_m^{\mathrm{P2G}} v_m^{\mathrm{G}} & f^{\mathrm{PV}} \eta^{\mathrm{P2G}} v_m^{\mathrm{P2G}} v_m^{\mathrm{G}} & \eta^{\mathrm{P2G}} v_m^{\mathrm{P2G}} v_m^{\mathrm{G}} & v_m^{G} + Q^{\mathrm{Gas}} \eta^{\mathrm{CHP,E}} v_m^{\mathrm{CHP}} v_m^{\mathrm{P2G}} \eta^{\mathrm{P2G}} v_m^{G} \end{bmatrix}}_{\boldsymbol{M}_{mm}} \underbrace{\begin{bmatrix} W_m^{\mathrm{WT}} \\ G_m^{\mathrm{PV}} \\ P_m^{\mathrm{BESS}} \\ V_m^{\mathrm{Tank}} \end{bmatrix}}_{\boldsymbol{S}_m} \tag{1}$$

where L_m^{E}, L_m^{H} and L_m^{Gas} denote electricity, heat, and gas loads of MG m; f^{WT} and f^{PV} are the generation functions of wind turbine (WT) and PV (Murty and Kumar, 2020); In Eq. (2), the off-diagonal element $\boldsymbol{M}_{ij}$ indicates the multi-energy resources delivered from the MG i to MG j and is equal to $\mathrm{diag}\{v_{ij}^{\mathrm{E}}, 0, v_{ij}^{\mathrm{G}}\}\boldsymbol{M}_{ii}$.

$$\begin{bmatrix} \boldsymbol{L}_1 \\ \boldsymbol{L}_2 \\ \vdots \\ \boldsymbol{L}_m \end{bmatrix} = \begin{bmatrix} \boldsymbol{M}_{11} & \boldsymbol{M}_{12} & \cdots & \boldsymbol{M}_{1m} \\ \boldsymbol{M}_{21} & \boldsymbol{M}_{22} & \cdots & \boldsymbol{M}_{2m} \\ \vdots & \vdots & \ddots & \vdots \\ \boldsymbol{M}_{m1} & \boldsymbol{M}_{m2} & \cdots & \boldsymbol{M}_{mm} \end{bmatrix} \begin{bmatrix} \boldsymbol{S}_1 \\ \boldsymbol{S}_2 \\ \vdots \\ \boldsymbol{S}_m \end{bmatrix} \tag{2}$$

In most cases, a MMGs contains various system dispatchable capacities, and these capacities can be utilized as external energy sources to provide energy for MGs' load. In this situation, the system dispatchable capacities can be considered as the external input terminals and integrated as an augmented column vector into the MMG coupling matrix. Thus, an extended coupling matrix for expressing the multi-

energy couplings and interactions within the whole MMG system is formulated as,

$$\begin{bmatrix} \boldsymbol{L}_1 \\ \boldsymbol{L}_2 \\ \vdots \\ \boldsymbol{L}_m \end{bmatrix} = \begin{bmatrix} \boldsymbol{M}_{11} & \boldsymbol{M}_{12} & \cdots & \boldsymbol{M}_{1m} & \boldsymbol{v}_{1,\mathrm{sys}} \\ \boldsymbol{M}_{21} & \boldsymbol{M}_{22} & \cdots & \boldsymbol{M}_{2m} & \boldsymbol{v}_{2,\mathrm{sys}} \\ \vdots & \vdots & \ddots & \vdots & \vdots \\ \boldsymbol{M}_{m1} & \boldsymbol{M}_{m2} & \cdots & \boldsymbol{M}_{mm} & \boldsymbol{v}_{m,\mathrm{sys}} \end{bmatrix} \begin{bmatrix} \boldsymbol{S}_1 \\ \boldsymbol{S}_2 \\ \vdots \\ \boldsymbol{S}_m \\ \boldsymbol{S}_{\mathrm{sys}} \end{bmatrix} \tag{3}$$

where $\boldsymbol{v}_{m,\mathrm{sys}}$ is equal to $\mathrm{diag}\{v_{m,\mathrm{sys}}^{\mathrm{E}}, 0, v_{m,\mathrm{sys}}^{\mathrm{G}}\}$, and $v_{m,\mathrm{sys}}^{\mathrm{E}}$ and $v_{m,\mathrm{sys}}^{\mathrm{G}}$ are dispatch factors of electricity and gas from system devices to MG m. The coupling matrix (3) is strongly nonlinear and high dimensional due to involving a large number of dispatch factors and controllable variables. Thus, a multi-step matrix decomposition technique is proposed to realize the linearization and dimensionality reduction of the coupling matrix. The first step is to decompose the matrix (3) into the MMG multi-energy coupling submatrix and dispatch submatrix of system capacities, as follows,

$$\begin{bmatrix} \boldsymbol{L}_1 \\ \boldsymbol{L}_2 \\ \vdots \\ \boldsymbol{L}_m \end{bmatrix} = \begin{bmatrix} \boldsymbol{M}_{11} & \boldsymbol{M}_{12} & \cdots & \boldsymbol{M}_{1m} & \boldsymbol{0} \\ \boldsymbol{M}_{21} & \boldsymbol{M}_{22} & \cdots & \boldsymbol{M}_{m} & \boldsymbol{0} \\ \vdots & \vdots & \ddots & \vdots & \vdots \\ \boldsymbol{M}_{m1} & \boldsymbol{M}_{m2} & \cdots & \boldsymbol{M}_{mm} & \boldsymbol{0} \end{bmatrix} \begin{bmatrix} \boldsymbol{S}_1 \\ \boldsymbol{S}_2 \\ \vdots \\ \boldsymbol{S}_m \\ \boldsymbol{S}_{\mathrm{sys}} \end{bmatrix} + \begin{bmatrix} \boldsymbol{0} & \boldsymbol{0} & \cdots & \boldsymbol{0} & \boldsymbol{v}_{1,\mathrm{sys}} \\ \boldsymbol{0} & \boldsymbol{0} & \cdots & \boldsymbol{0} & \boldsymbol{v}_{2,\mathrm{sys}} \\ \vdots & \vdots & \ddots & \vdots & \vdots \\ \boldsymbol{0} & \boldsymbol{0} & \cdots & \boldsymbol{0} & \boldsymbol{v}_{m,\mathrm{sys}} \end{bmatrix} \begin{bmatrix} \boldsymbol{S}_1 \\ \boldsymbol{S}_2 \\ \vdots \\ \boldsymbol{S}_m \\ \boldsymbol{S}_{\mathrm{sys}} \end{bmatrix} \tag{4}$$

Reorganizing (4), it can be rewritten as,

$$\begin{bmatrix} \boldsymbol{L}_1 \\ \boldsymbol{L}_2 \\ \vdots \\ \boldsymbol{L}_m \end{bmatrix} = \begin{bmatrix} \boldsymbol{M}_{11} & \boldsymbol{M}_{12} & \cdots & \boldsymbol{M}_{1m} \\ \boldsymbol{M}_{21} & \boldsymbol{M}_{22} & \cdots & \boldsymbol{M}_{m} \\ \vdots & \vdots & \ddots & \vdots \\ \boldsymbol{M}_{m1} & \boldsymbol{M}_{m2} & \cdots & \boldsymbol{M}_{mm} \end{bmatrix} \begin{bmatrix} \boldsymbol{S}_1 \\ \boldsymbol{S}_2 \\ \vdots \\ \boldsymbol{S}_m \end{bmatrix} + \begin{bmatrix} \boldsymbol{v}_{1,\mathrm{sys}} \boldsymbol{S}_{\mathrm{sys}} \\ \boldsymbol{v}_{2,\mathrm{sys}} \boldsymbol{S}_{\mathrm{sys}} \\ \vdots \\ \boldsymbol{v}_{m,\mathrm{sys}} \boldsymbol{S}_{\mathrm{sys}} \end{bmatrix} \tag{5}$$

The second step aims to decompose the MMG multi-energy coupling matrix into the multi-energy coupling submatrix and the multi-energy exchange submatrix. In a MMG system, the energy exchanging with other MGs can be equivalent to virtual energy sources in the MG's input side, and thus the off-diagonal element $\boldsymbol{M}_{ij}$ is substituted with the input vector $\boldsymbol{S}_i^{\mathrm{ex}}$. Eq. (5) can be reformulated as,

$$\begin{bmatrix} \boldsymbol{L}_1 \\ \boldsymbol{L}_2 \\ \vdots \\ \boldsymbol{L}_m \end{bmatrix} = \begin{bmatrix} \begin{bmatrix} \boldsymbol{M}_{11} & \boldsymbol{I} \end{bmatrix} & \boldsymbol{0} & \cdots & \boldsymbol{0} \\ \boldsymbol{0} & \begin{bmatrix} \boldsymbol{M}_{22} & \boldsymbol{I} \end{bmatrix} & \cdots & \boldsymbol{0} \\ \vdots & \vdots & \ddots & \vdots \\ \boldsymbol{0} & \boldsymbol{0} & \boldsymbol{0} & \begin{bmatrix} \boldsymbol{M}_{mm} & \boldsymbol{I} \end{bmatrix} \end{bmatrix} \begin{bmatrix} \begin{bmatrix} \boldsymbol{S}_1 \\ \boldsymbol{S}_1^{\mathrm{ex}} \end{bmatrix} \\ \begin{bmatrix} \boldsymbol{S}_1 \\ \boldsymbol{S}_2^{\mathrm{ex}} \end{bmatrix} \\ \vdots \\ \begin{bmatrix} \boldsymbol{S}_1 \\ \boldsymbol{S}_m^{\mathrm{ex}} \end{bmatrix} \end{bmatrix} + \begin{bmatrix} \boldsymbol{v}_{1,\mathrm{sys}} \boldsymbol{S}_{\mathrm{sys}} \\ \boldsymbol{v}_{2,\mathrm{sys}} \boldsymbol{S}_{\mathrm{sys}} \\ \vdots \\ \boldsymbol{v}_{m,\mathrm{sys}} \boldsymbol{S}_{\mathrm{sys}} \end{bmatrix} \tag{6}$$

where $\boldsymbol{S}_m^{\mathrm{ex}} = [\boldsymbol{P}_{m,t}^{\mathrm{rec,E}} - \boldsymbol{P}_{m,t}^{\mathrm{send,E}}, 0, \boldsymbol{V}_{m,t}^{\mathrm{rec,G}} - \boldsymbol{V}_{m,t}^{\mathrm{send,G}}]^{\mathrm{T}}$; $\mathbf{P}_{m,t}^{\mathrm{send,E}}$ and $\boldsymbol{V}_{m,t}^{\mathrm{send,G}}$ denote energy carries delivered from MG m to other MGs; $\mathbf{P}_{m,t}^{\mathrm{send,E}} = [P_{m,1,t}^{\mathrm{E}}, P_{m,2,t}^{\mathrm{E}}, \cdots, P_{m,M,t}^{\mathrm{E}}]^{\mathrm{T}}$ and $\boldsymbol{V}_{m,t}^{\mathrm{send,G}} = [V_{m,1,t}^{\mathrm{E}}, V_{m,2,t}^{\mathrm{E}}, \cdots, V_{m,M,t}^{\mathrm{E}}]^{\mathrm{T}}$; $\boldsymbol{P}_{m,t}^{\mathrm{rec,E}}$ and $\boldsymbol{V}_{m,t}^{\mathrm{rec,G}}$ indicate energy sources purchased from other MGs; $\boldsymbol{P}_{m,t}^{\mathrm{rec,E}} = [P_{1,m,t}^{\mathrm{E}}, P_{2,m,t}^{\mathrm{E}}, \cdots, P_{M,m,t}^{\mathrm{E}}]^{\mathrm{T}}$ and $\boldsymbol{V}_{m,t}^{\mathrm{rec,G}} = [V_{1,m,t}^{\mathrm{E}}, V_{2,m,t}^{\mathrm{E}}, \cdots, V_{M,m,t}^{\mathrm{E}}]^{\mathrm{T}}$.

The third step utilizes a state variable-based approach in (Shao et al., 2017) to reduce the nonlinearity caused by dispatch factors. The outputs of the electric boiler, furnace, CHP and P2G system would be represented as $Q_{m,t}^{\mathrm{Boi}}$, $Q_{m,t}^{\mathrm{Fur}}$, $P_{m,t}^{\mathrm{CHP}}$, $V_{m,t}^{\mathrm{P2G}}$ without introducing dispatch factors. Combining these state variables with the original input vector $\boldsymbol{S}_m$ in (1), an extended variable vector $\boldsymbol{S}_m^{'}$ is formulated, and the matrix $\boldsymbol{M}_{m,m}$ is further extended to a sparser and linear coupling matrix $\boldsymbol{M}_{m,m}^{'}$, as shown in (7). The detailed process of this step is shown in Appendix A.

$$\underbrace{\begin{bmatrix} L_m^E \\ L_m^H \\ L_m^{\mathrm{Gas}} \end{bmatrix}}_{\boldsymbol{L}_m} = \underbrace{\begin{bmatrix} 1 & 1 & -/\eta^{\mathrm{P2G}} & 1 & 0 & 1 & -1/\eta^{\mathrm{Boi}} & 0 \\ 0 & 0 & 0 & 0 & 1 & \eta^{\mathrm{CHP,H}}/\eta^{\mathrm{CHP,E}} & 1 & 0 \\ 0 & 0 & 1 & 0 & -1/\eta^{\mathrm{Fur}}Q^{\mathrm{Gas}} & -1/\eta^{\mathrm{CHP,E}}Q^{\mathrm{Gas}} & 0 & 1 \end{bmatrix}}_{\boldsymbol{M}_{m,m}^{'}} \underbrace{\begin{bmatrix} P^{\mathrm{WT}} \\ P^{\mathrm{PV}} \\ V_{m,t}^{\mathrm{P2G}} \\ P_{m,t}^{\mathrm{BESS}} \\ Q_{m,t}^{\mathrm{Fur}} \\ P_{m,t}^{\mathrm{CHP}} \\ Q_{m,t}^{\mathrm{Boi}} \\ V_{m,t}^{\mathrm{Tank}} \end{bmatrix}}_{\boldsymbol{S}_m^{'}} \tag{7}$$

Combining (6) and (7), the coupling matrix of the whole MMGs system can be decomposed into the sum of three linear and sparse submatrices for efficient computational iterations, where the first submatrix represents the multi-energy coupling within MGs, the second submatrix indicates multi-energy exchanges among MMGs and the third submatrix represents the allocation of system capacities. Based on the obtained (8), an interactive tri-level multi-energy management strategy is proposed to coordinate the operation of the MMG system.

$$\begin{bmatrix} \boldsymbol{L}_1 \\ \boldsymbol{L}_2 \\ \vdots \\ \boldsymbol{L}_m \end{bmatrix} = \underbrace{\begin{bmatrix} \boldsymbol{M}_{11}'\boldsymbol{S}_1' \\ \boldsymbol{M}_{22}'\boldsymbol{S}_2' \\ \vdots \\ \boldsymbol{M}_{mm}'\boldsymbol{S}_m' \end{bmatrix}}_{\text{submatrix 1}} + \underbrace{\begin{bmatrix} \boldsymbol{IS}_1^{\mathrm{ex}} \\ \boldsymbol{IS}_2^{\mathrm{ex}} \\ \vdots \\ \boldsymbol{IS}_m^{\mathrm{ex}} \end{bmatrix}}_{\text{submatrix 2}} + \underbrace{\begin{bmatrix} \boldsymbol{v}_{1,\mathrm{sys}}\boldsymbol{S}_{\mathrm{sys}} \\ \boldsymbol{v}_{2,\mathrm{sys}}\boldsymbol{S}_{\mathrm{sys}} \\ \vdots \\ \boldsymbol{v}_{m,\mathrm{sys}}\boldsymbol{S}_{\mathrm{sys}} \end{bmatrix}}_{\text{submatrix 3}} \tag{8}$$

3 Interactive tri-level multi-energy management strategy

3.1 Assumptions

Before formulating the proposed strategy for MMGs, several assumptions are made as follows:

- Transients in energy networks and their components are not considered, since the duration of transient is extremely short compared with the hourly time resolution over a 24-hour scheduling horizon.
- The capacities of external energy networks are large enough to meet the electricity and gas demand of MMGs during the necessary time, and the surplus energy sources of MMGs can also be integrated into energy networks without other stability issues.
- The communication network is assumed to be reliable, scalable and fast to ensure the real-time data exchange among MMGs.

3.2 Lower level of MMGMEM

1) Objective Function: This level aims to optimally manage the multi-energy conversion and storage in each MG considering the volatility of RDG outputs and time-varying multi-energy demands. The optimization objective of this level is to minimize the operation cost of each MG $SC_{m,t}$, including energy procurement costs, start-up/shut-down costs, and battery degradation costs, as follows:

$$\begin{aligned} SC_{m,t} = {} & (C_t^{\text{buy,Gas}} V_{m,t}^{\text{short,Gas}} - C_t^{\text{sell,Gas}} V_{m,t}^{\text{sur,Gas}})\Delta t + (C_t^{\text{buy,E}} P_{m,t}^{\text{short,E}} - C_t^{\text{sell,E}} P_{m,t}^{\text{sur,E}})\Delta t + \\ & \sum_{i \in \boldsymbol{I}_{m,3}} (v_t(1-v_{t-1})C_{m,i}^{\text{CHP}} + \sum_{i \in \boldsymbol{I}_{m,2}} \omega_t(1-\omega_{t-1})C_{m,i}^{\text{Boi}} + \sum_{i \in \boldsymbol{I}_{m,4}} \tau_t(1-\tau_{t-1})C_{m,i}^{\text{Fur}} + \sum_{i \in \boldsymbol{I}_{m,5}} \mu^{\text{BESS}}(P_{m,i,t}^{\text{BESS,dis}} + P_{m,i,t}^{\text{BESS,ch}})\Delta t \end{aligned} \quad (9)$$

where μ^{BESS} is the amortized cost of BESS charging/discharging over the lifetime which is related to the capital cost of batteries, the reference depth-of-discharge, and the number of cycles (Xu et al., 2020). In this paper, a scenario-based stochastic scheduling with rolling horizon procedures is performed to tackle the uncertainties (Langer and Volling, 2020). Every rolling optimization step makes decisions for the current time slot and also looks forward to the remaining time slots considering uncertainties of renewable generations and multi-energy loads in future time slots. The objective function is to minimize the MG's operation cost of the current time slot *t* plus the expected cost of all future scenarios, as follows,

$$\min \left\{ SC_{m,t_0} + \sum_{s=1}^{N_s} \rho_s \left(\sum_{t=t_0+\Delta t}^{t_0+T} SC_{m,t,s} \right) \right\} \quad (10)$$

where N_s is the total number of scenarios; ρ_s denotes the probability of scenario *s*, and $\sum_{s=1}^{NS} \rho_s = 1$. $SC_{m,t,s}$ represents the operation cost of MG *m* under scenario *s* at the current time slot *t*. The prediction horizon *T* represents the length of future time slots, and the control horizon Δt indicates the length of time slot over which the previous scheduling decision was executed before starting a new optimization run.

2) Energy balance constraints: The amount of multi-energy demand for each MG should be equal to the sum of the corresponding energy supply, as follows,

$$\boldsymbol{L}_{m,t} = \boldsymbol{M}'_{mm,t} \boldsymbol{S}'_{m,t} + \boldsymbol{E}_{m,t} \quad (11)$$

where $\boldsymbol{M}'_{m,m}\boldsymbol{S}'_{m,t}$ is the energy hub model in submatrix 1, as described in (8). The shortage/surplus amount of energy in the current time slot is $\boldsymbol{E}_{m,t} = [P_{m,t}^{\text{short,E}} - P_{m,t}^{\text{sur,E}}, 0, V_{m,t}^{\text{short,Gas}} - V_{m,t}^{\text{sur,Gas}}]^{\text{T}}$.

3) Converters and Storages constraints: Objective (10) is subjected to constraints of multi-energy conversion and storage devices. Eq. (12) shows the lower and upper bounds of P2G outputs. (13)-(16) indicate constraints for the state of charge (SOC) and outputs of BESS. (17)-(20) show constraints for the SOC and outputs of the gas storage tank, and (21)-(23) denote the constraints of CHP outputs. (24) and (25) show constraints of thermal power outputs of the electric boiler and furnace.

$$V_{m,i}^{\text{P2G,min}} \le V_{m,i,t}^{\text{P2G}} \le V_{m,i}^{\text{P2G,max}} \quad i \in I_{m,1} \tag{12}$$

$$SOC_{m,i,t}^{\text{BESS}} = SOC_{m,i,t\text{-}\Delta t}^{\text{BESS}} + \frac{\eta^{\text{ch}} P_{m,i,t\text{-}\Delta t}^{\text{BESS,ch}} \Delta t}{E_{m,i}^{R}} - \frac{P_{m,i,t\text{-}\Delta t}^{\text{BESS,dis}} \Delta t}{\eta^{\text{dis}} E_{m,i}^{R}} \quad i \in I_{m,5} \tag{13}$$

$$SOC_{m,i}^{\text{BESS,min}} \le SOC_{m,i,t}^{\text{BESS}} \le SOC_{m,i}^{\text{BESS,max}} \quad i \in I_{m,5} \tag{14}$$

$$\begin{cases} 0 \le P_{m,i,t}^{\text{BESS,ch}} \le P_{m,i}^{\text{BESS,ch,max}} \delta_{m,i,t} \\ 0 \le P_{m,i,t}^{\text{BESS,dis}} \le P_{m,i}^{\text{BESS,dis,max}} \varphi_{m,i,t} \end{cases} \quad i \in I_{m,5} \tag{15}$$

$$\delta_{m,i,t} + \varphi_{m,i,t} \le 1 \quad \delta_{m,i,t}, \varphi_{m,i,t} \in \{0,1\}, i \in I_{m,5} \tag{16}$$

$$SOC_{m,i,t}^{\text{Tank}} = SOC_{m,i,t\text{-}\Delta t}^{\text{Tank}} + \frac{V_{m,i,t\text{-}\Delta}^{\text{Tank,ch}} \Delta t}{V_{m,i}^{R}} - \frac{V_{m,i,t\text{-}\Delta}^{\text{Tank,dis}} \Delta t}{V_{m,i}^{R}} \quad i \in I_{m,6} \tag{17}$$

$$SOC_{m,i}^{\text{Tank,min}} \le SOC_{m,i,t}^{\text{Tank}} \le SOC_{m,i}^{\text{Tank,max}} \quad i \in I_{m,6} \tag{18}$$

$$\begin{cases} 0 \le V_{m,i,t}^{\text{Tank,ch}} \le V_{m,i}^{\text{Tank,ch,max}} \psi_{m,i,t} \\ 0 \le V_{m,i,t}^{\text{Tank,dis}} \le V_{m,i}^{\text{Tank,dis,max}} \phi_{m,i,t} \end{cases} \quad i \in I_{m,6} \tag{19}$$

$$\psi_{m,i,t} + \phi_{m,i,t} \le 1 \quad \psi_{m,i,t}, \phi_{m,i,t} \in \{0,1\}, i \in I_{m,6} \tag{20}$$

$$-v_{m,i,t} P_{m,i}^{\text{CHP,min}} \le P_{m,i,t}^{\text{CHP}} \le v_{m,i,t} P_{m,i}^{\text{CHP,max}} \quad i \in I_{m,3} \tag{21}$$

$$-v_{m,i,t} H_{m,i}^{\text{CHP,min}} \le \frac{P_{m,i,t}^{\text{CHP}} \eta_{m,i}^{\text{CHP,H}}}{\eta_{m,i}^{\text{CHP,E}}} \le v_{m,i,t} H_{m,i}^{\text{CHP,max}} \quad i \in I_{m,3} \tag{22}$$

$$-P_{m,i}^{\text{CHP,ramp}} \le P_{m,i,t}^{\text{CHP}} - P_{m,i,t-\Delta t}^{\text{CHP}} \le P_{m,i}^{\text{CHP,ramp}} \quad i \in I_{m,3} \tag{23}$$

$$Q_{m,i}^{\text{Boi,min}} \le Q_{m,i,t}^{\text{Boi}} \le Q_{m,i}^{\text{Boi,max}} \quad i \in I_{m,2} \tag{24}$$

$$Q_{m,i}^{\text{Fur,min}} \le Q_{m,i,t}^{\text{Fur}} \le Q_{m,i}^{\text{Fur,max}} \quad i \in I_{m,4} \tag{25}$$

After completing local optimization by each MG-EMS, the surplus/shortage amount of energy is determined, and the upper bounds of increasable energy for each MG will also be calculated. Then, these determined values from the current time slots t_0 to the future time slot $t_0 + T$, and the unit cost of increasable energy will be transmitted to the CEMS. Moreover, CEMS will contract with MG-EMSs

participating in global optimization to ensure that each MG-EMSs report its true information, and the third party inspection namely random audit in (Zhang and Zhao, 2012) is introduced into the contract. If the MG-EMS reports the untruthful data to CEMS, it will face a risk of being levied a hefty fine.

3.3 Upper level of MMGMEM

1) Objective Function: Based on the information obtained from each MG-EMS, this level performs global optimization for the optimal scheduling of system dispatchable capacities, and then the amount of energy to be traded with multi-energy networks is determined. The objective function is developed to minimize the sum of the system operation cost at current time t_0, the accumulated system operation cost determined by previous multi-energy scheduling, and the future operation cost from time slot $t_0+\Delta t$ to the end of time slot t_0+T, as follows,

$$\min CSC_{t_0}+\sum_{t=1}^{t_0-\Delta t}(CSC_t)+\sum_{t=t_0+\Delta t}^{t_0+T}(CSC_t) \tag{26}$$

$$CSC_t = CDC_t + CBC_t + CAC_t \tag{27}$$

$$CDC_t = a(P_t^{\mathrm{CCDG}})^2 + b(P_t^{\mathrm{CCDG}}) + c + u_t(1-u_{t-1})C^{\mathrm{CCDG}} + \mu^{\mathrm{CBESS}}(P_t^{\mathrm{CBESS,dis}}+P_t^{\mathrm{CBESS,ch}})\Delta t \tag{28}$$

$$CBC_t = (C_t^{\mathrm{buy,Gas}}V_t^{\mathrm{buy,Gas}} - C_t^{\mathrm{sell,Gas}}V_t^{\mathrm{sell,Gas}})\Delta t + (C_t^{\mathrm{buy,E}}P_t^{\mathrm{buy,E}} - C_t^{\mathrm{sell,E}}P_t^{\mathrm{sell,E}})\Delta t \tag{29}$$

$$CAC_t = \sum_{m=1}^{M}\sum_{i=1}^{I}(C_{m,i}^{\mathrm{Increase,P}}\Delta P_{m,i,t} + C_{m,i}^{\mathrm{Increase,G}}\Delta V_{m,i,t})\Delta t \tag{30}$$

where the energy consumption cost of CCDG is related to outputs of CCDG P_t^{CCDG}, and a quadratic function in (Hao et al., 2018) is adopted. CDC_t is the sum of the generation cost of CCDG and the degradation cost of CBESS; CBC_t is the energy procurement cost, and CAC_t denotes the cost for increasing energy outputs.

2) System constraints: The outputs of CCDG are limited within its allowed capacities and ramp rates. The charging/discharging power of CBESS should be limited within the maximum threshold $P^{\mathrm{CBESS,ch,max}}/P^{\mathrm{CBESS,dis,max}}$, and the SOC of CBESS shall be limited in an allowable range. Besides, The CEMS ensures that the energy adjustment is less than the maximum constraints of increasable capabilities.

$$u_t P^{\mathrm{CCDG,min}} \le P_t^{\mathrm{CCDG}} \le u_t P^{\mathrm{CCDG,max}} \quad u_t \in \{0,1\} \tag{31}$$

$$-R^{\mathrm{CCDG,down}} \le P_t^{\mathrm{CCDG}} - P_{t-1}^{\mathrm{CCDG}} \le R^{\mathrm{CCDG,up}} \tag{32}$$

$$SOC_t^{\mathrm{CBESS}} = SOC_{t-\Delta t}^{\mathrm{CBESS}} + \frac{\eta^{\mathrm{ch}}P_{t-\Delta t}^{\mathrm{CBESS,ch}}\Delta t}{E^{\mathrm{CBESS,R}}} - \frac{P_{t-\Delta t}^{\mathrm{CBESS,dis}}\Delta t}{\eta^{\mathrm{dis}}E^{\mathrm{CBESS,R}}} \tag{33}$$

$$SOC_{\min} \le SOC_{m,t}^{\mathrm{CBESS}} \le SOC_{\max} \tag{34}$$

$$\begin{cases} 0 \le P_t^{\text{CBESS,ch}} \le P^{\text{CBESS,ch,max}} \delta_t \\ 0 \le P_t^{\text{CBESS,dis}} \le P^{\text{CBESS,dis,max}} \varphi_t \end{cases} \tag{35}$$

$$\delta_t + \varphi_t \le 1 \quad \delta_t, \varphi_t \in \{0,1\} \tag{36}$$

$$0 \le \Delta P_{m,i,t} \le \Delta P_{m,i,t}^{\max} \tag{37}$$

$$0 \le \Delta V_{m,i,t} \le \Delta V_{m,i,t}^{\max} \tag{38}$$

Besides, the equality constraints for power and gas flow balance are enforced as,

$$P_t^{\text{CCDG}} + P_t^{\text{CBESS,dis}} - P_t^{\text{CBESS,ch}} + P_t^{\text{buy,E}} - P_t^{\text{sell,E}} + \sum_{m=1}^{M} \sum_{i=1}^{I} \Delta P_{m,i,t} = \sum_{m=1}^{M} (P_{m,t}^{\text{short,E}} - P_{m,t}^{\text{sur,E}}) \tag{39}$$

$$V_t^{\text{buy,Gas}} - V_t^{\text{sell,Gas}} + \sum_{m=1}^{M} \sum_{i=1}^{I} \Delta V_{m,i,t} = \sum_{m=1}^{M} (V_{m,t}^{\text{short,Gas}} - V_{m,t}^{\text{sur,Gas}}) \tag{40}$$

After completing the global optimization of the MMG system, the amount of energy trading with electricity and gas networks, generation outputs of system devices and the amount of energy generation to be increased are determined, and then they are submitted to the middle level.

3.4 Middle level of MMGMEM

During the energy allocation period, each MG wants to exchange as much energy as possible with the connected MGs rather than trading with the energy networks to pursue its benefits, and thus competitive behaviors appear among MMGs. The competitive behaviors often are contrary to the best benefits of global MMGs, and the overall benefits may be unfairly distributed among MMGs. In this way, the willingness of some MGs to proactively participate in multi-energy sharing will be significantly decreased (Jafari et al., 2020b). Besides, due to self-interest competitive behaviors, the flexibility of multi-energy conversion and interactions within MMGs will be hard to fully leverage for achieving the best load balancing performance, and the extremely non-uniform energy demand may also occur resulting in energy networks failure, as all MGs buy energy at a low price and sell energy at a high price (Zhou et al., 2020a). This level will further correct the energy scheduling decisions from the upper level to allocate electricity and gas from system capacities and multi-energy networks to each MG, and the multi-energy sharing among MGs can be coordinated based on the many-criteria optimality model (Farina and Amato, 2004).

1) Many-objective Optimization Function: To schedule the benefit-maximal operation of each MG, the MMG multi-energy sharing problem in this level is formulated to simultaneously maximize benefits of heterogeneous MGs with different multi-energy converters and storages, as follows,

$$\max \ F = (f_1, f_2, \ldots f_m, \ldots, f_{\text{M}}) \tag{41}$$

where f_m indicates its benefit, including current benefits, accumulated benefits from previous multi-energy scheduling, and future benefits from time slot $t_0 + \Delta t$ to the end of scheduling horizon, as follows,

$$f_m = RBC_{m,t_0} + RTC_{m,t_0} - RAC_{m,t_0} + \sum_{t=1}^{t_0-\Delta t}(RBC_{m,t} + RTC_{m,t} - RAC_{m,t}) + \sum_{t=t_0+\Delta t}^{t_0+T}(RBC_{m,t} + RTC_{m,t} - RAC_{m,t}) \quad (42)$$

$$RBC_{m,t} = (\mathrm{y}_{m,t}^{\mathrm{G}} C_t^{\mathrm{sell,Gas}} V_{m,t}^{\mathrm{sell,Gas}} - x_{m,t}^{\mathrm{G}} C_t^{\mathrm{buy,Gas}} V_{m,t}^{\mathrm{buy,Gas}})\Delta t + (\mathrm{y}_{m,t}^{\mathrm{E}} C_t^{\mathrm{sell,E}} P_{m,t}^{\mathrm{sell,E}} - x_{m,t}^{\mathrm{E}} C_t^{\mathrm{buy,E}} P_{m,t}^{\mathrm{buy,E}})\Delta t \quad (43)$$

$$RTC_{m,t} = C^{\mathrm{sr,e}}(\boldsymbol{e}_m^{\mathrm{T}} \boldsymbol{A} \boldsymbol{P}_{m,t}^{\mathrm{send,E}} - \boldsymbol{e}_m^{\mathrm{T}} \boldsymbol{A}^{\mathrm{T}} \boldsymbol{P}_{m,t}^{\mathrm{rec,E}})\Delta t + C^{\mathrm{sr,g}}(\boldsymbol{e}_m^{\mathrm{T}} \boldsymbol{B} \boldsymbol{V}_{m,t}^{\mathrm{send,G}} - \boldsymbol{e}_m^{\mathrm{T}} \boldsymbol{B}^{\mathrm{T}} \boldsymbol{V}_{m,t}^{\mathrm{rec,G}})\Delta t \quad (44)$$

$$RAC_{m,t} = \sum_{i \in I_{m,3}, I_{m,5}} C_{m,i}^{\mathrm{Increase,P}} \Delta P_{m,i,t} + \sum_{i \in I_{m,1}, I_{m,6}} C_{m,i}^{\mathrm{Increase,G}} \Delta V_{m,i,t} \quad (45)$$

where $RBC_{m,t}$ is the benefit of energy trading with the energy networks; $RTC_{m,t}$ represents the benefit from the energy exchange with other MGs; $RAC_{m,t}$ denotes the cost for increasing energy generation; $\boldsymbol{e}_m^{\mathrm{T}} \boldsymbol{A} \boldsymbol{P}_{m,t}^{\mathrm{send,E}}$, $\boldsymbol{e}_m^{\mathrm{T}} \boldsymbol{A}^{\mathrm{T}} \boldsymbol{P}_{m,t}^{\mathrm{rec,E}}$, $\boldsymbol{e}_m^{\mathrm{T}} \boldsymbol{B} \boldsymbol{V}_{m,t}^{\mathrm{send,G}}$ and $\boldsymbol{e}_m^{\mathrm{T}} \boldsymbol{B}^{\mathrm{T}} \boldsymbol{V}_{m,t}^{\mathrm{rec,G}}$ are the total amount of power and gas sold/purchased to/from other MGs at time slot *t* for MG *m*, respectively; $\boldsymbol{e}_m$ is the *m*th column of the $M \times M$ identity matrix; $\boldsymbol{A}$ and $\boldsymbol{B}$ are adjacency matrix $[a_{m,n}]_{M \times M}$ and $[b_{m,n}]_{M \times M}$, where element $a_{m,n}$ represents the power line connecting MG *m* and MG *n*, and $b_{m,n}$ indicates a gas pipeline between MG *m* and MG *n*; If there exists an electrical line connection between MG *m* and MG *n*, element $a_{m,n}$ is equal to 1, and 0 otherwise; It is noted that prices of energy exchange $C^{\mathrm{sr,e}}$ and $C^{\mathrm{sr,g}}$ play an important role to encourage MGs with excess energy to send energy to neighboring MGs, and their values are obtained from (Jadhav et al., 2019). The problem in (41)-(45) with four or more objectives is generally defined as many-objective optimization (Zhou et al., 2020b). As each MG pursues its benefit maximization, the utility functions of MMGs are always contradictory and competitive. Hence, a many-criteria optimality model is developed to identify the best compromise solution with well-distributed tradeoff benefits for all MGs' objectives, and thus benefits from multi-energy sharing can be impartially allocated among MMGs.

2) Energy Balance Constraints: The constraints of power and gas balance in MG *m* are expressed as (46) and (47), while (48) and (49) express that the sum of the exchanged electricity and gas among MMGs should be equal zero. Moreover, the total amount of energy trading and outputs of system devices determined by the upper level should be considered in constraints, and the electricity and gas purchased/sold from/to energy networks and system devices for all MGs should satisfy (48)-(51).

$$P_{m,t}^{\mathrm{sell,E}} + \boldsymbol{e}_m^{\mathrm{T}} \boldsymbol{A} \boldsymbol{P}_{m,t}^{\mathrm{send,E}} + P_{m,t}^{\mathrm{short,E}} = P_{m,t}^{\mathrm{buy,E}} + \boldsymbol{e}_m^{\mathrm{T}} \boldsymbol{A}^{\mathrm{T}} \boldsymbol{P}_{m,t}^{\mathrm{rec,E}} + P_{m,t}^{\mathrm{sur,E}} + \sum_{i \in I_{m,3}, I_{m,5}} \Delta P_{m,i,t} \quad (46)$$

$$V_{m,t}^{\mathrm{sell,Gas}} + \boldsymbol{e}_m^{\mathrm{T}} \boldsymbol{B} \boldsymbol{V}_{m,t}^{\mathrm{send,G}} + V_{m,t}^{\mathrm{short,gas}} = V_{m,t}^{\mathrm{buy,Gas}} + \boldsymbol{e}_m^{\mathrm{T}} \boldsymbol{B}^{\mathrm{T}} \boldsymbol{V}_{m,t}^{\mathrm{rec,G}} + V_{m,t}^{\mathrm{sur,Gas}} + \sum_{i \in I_{m,1}, I_{m,6}} \Delta V_{m,i,t} \quad (47)$$

$$\sum_{m \in M} \boldsymbol{e}_m^{\mathrm{T}} \boldsymbol{A}^{\mathrm{T}} \boldsymbol{P}_{m,t}^{\mathrm{rec,E}} - \sum_{m \in M} \boldsymbol{e}_m^{\mathrm{T}} \boldsymbol{A} \boldsymbol{P}_{m,t}^{\mathrm{send,E}} = 0 \quad (48)$$

$$\sum_{m\in M} \boldsymbol{e}_m^{\mathrm{T}} \boldsymbol{B}^{\mathrm{T}} \boldsymbol{V}_{m,t}^{\mathrm{rec,G}} - \sum_{m\in M} \boldsymbol{e}_m^{\mathrm{T}} \boldsymbol{B} \boldsymbol{V}_{m,t}^{\mathrm{send,G}} = 0 \tag{49}$$

$$\sum_{m\in M} P_{m,t}^{\mathrm{buy,E}} = P_t^{\mathrm{buy,E}} + P_t^{\mathrm{CCDG}} + P_t^{\mathrm{CBESS,dis}} \tag{50}$$

$$\sum_{m\in M} P_{m,t}^{\mathrm{sell,E}} = P_t^{\mathrm{sell,E}} + P_t^{\mathrm{CBESS,ch}} \tag{51}$$

$$\sum_{m\in M} V_{m,t}^{\mathrm{buy,Gas}} = V_t^{\mathrm{buy,Gas}} \tag{52}$$

$$\sum_{m\in M} V_{m,t}^{\mathrm{sell,Gas}} = V_t^{\mathrm{sell,Gas}} \tag{53}$$

3) Energy security Constraints: The constraints for the capacity of gas pipelines are described as (54)-(55), and the limitation of electrical line capacity is denoted as (56)-(57). Especially, the amount of electricity and gas in a MMGs that can be traded with energy networks is assumed to be unlimited as follows,

$$0 \le \boldsymbol{e}_m^{\mathrm{T}} \boldsymbol{A} \boldsymbol{P}_{m,t}^{\mathrm{send,E}} \le x_{m,t}^{\mathrm{E}} P_{\max}^{\mathrm{line}} \tag{54}$$

$$0 \le \boldsymbol{e}_m^{\mathrm{T}} \boldsymbol{A}^{\mathrm{T}} \boldsymbol{P}_{m,t}^{\mathrm{rec,E}} \le (1 - x_{m,t}^{\mathrm{E}}) P_{\max}^{\mathrm{line}} \tag{55}$$

$$0 \le \boldsymbol{e}_m^{\mathrm{T}} \boldsymbol{B} \boldsymbol{V}_{m,t}^{\mathrm{send,G}} \le x_{m,t}^{\mathrm{Gas}} V_{\max}^{\mathrm{pipeline}} \tag{56}$$

$$0 \le \boldsymbol{e}_m^{\mathrm{T}} \boldsymbol{B}^{\mathrm{T}} \boldsymbol{V}_{m,t}^{\mathrm{rec,G}} \le (1 - x_{m,t}^{\mathrm{Gas}}) V_{\max}^{\mathrm{pipeline}} \tag{57}$$

where $x_{m,t}^{\mathrm{E}}$ and $x_{m,t}^{\mathrm{Gas}}$ denote the direction of transmission of energy. $x_{m,t}^{\mathrm{E}}$=1 represents that MG *m* exports its surplus electricity to other MGs; otherwise, $x_{m,t}^{\mathrm{E}}$=0. The definition of gas flow is the same.

4) Many-Criteria Optimality Methodology: The MMGMEM in the lower and upper level is modeled as a mixed-integer linear programming problem and a mixed-integer quadratic programming problem respectively, which can be solved by the CPLEX solver in the freely available YALMIP toolbox (Xu et al., 2020). In the middle level, the EMOHT algorithm in (Zhou et al., 2020b) is used to solve many-objective optimization problems. At each iteration of EMOHT, the corner sort is employed to identify *H* extreme non-dominated solutions, and a set of extreme points is used to construct a hyperplane, as follows,

$$\gamma_1 \cdot f_1 + \gamma_2 \cdot f_2 + \ldots + \gamma_m \cdot f_m + \ldots + \gamma_M \cdot f_M = 1 \tag{58}$$

where $(\gamma_1, \gamma_2, \ldots, \gamma_M)$ is the unit normal vector of the hyperplane; $f_1, f_2, \ldots, f_M$ are the coordinates of extreme points to indicate many-objective functions, and $z=(f_{1,\min}, f_{2,\min}, \ldots, f_{M,\min})$ is the ideal point. Therefore, each solution can be normalized with $\bar{f}_m = (f_m - f_{m,min})/(I_m - f_{m,min})$. Here, the ideal point is normalized to $z^* = (0, 0, \ldots, 0)$. The coordinates of solutions can then be projected from many-objective hypercube to the hyperplane by using $f_m' = \bar{f}_m/(\bar{f}_1 + \bar{f}_2 + \cdots + \bar{f}_M)$.

On the hyperplane, a set of symmetric reference points is generated by leveraging the normal boundary intersection. The solution projection and classification for a three-objective problem is illustrated in Fig. 3.

solution X is projected to the solution X' on the normalized hyperplane. The projected solutions can be divided into several groups according to these generated reference points. Then, two independent distance measures are utilized by EMOHT to select and store elitist solutions in the population, and the two distances are linearly combined into an integrated measure, as follows,

$$d_1 = \sqrt{\sum_{m=1}^{M} (\bar{f}_m)^2} \tag{59}$$

$$d_2 = \sqrt{\sum_{m=1}^{M} (f'_m - x_{m,n})^2} \tag{60}$$

$$d = \omega \cdot \frac{d_1 - d_{1,\min}}{d_{1,\max} - d_{1,\min}} + (1-\omega) \cdot \frac{d_2 - d_{2,\min}}{d_{2,\max} - d_{2,\min}} \tag{61}$$

where d_1 is the distance between the solution and ideal point for controlling the convergence of the algorithm, while d_2 is the Euclidean distance between the reference point and the projected solution for controlling the population diversity. Weighting factor ω represents the trade-off between convergence and diversity, and the value of ω is set as 1-$(iter/iter_{\max})^2$.

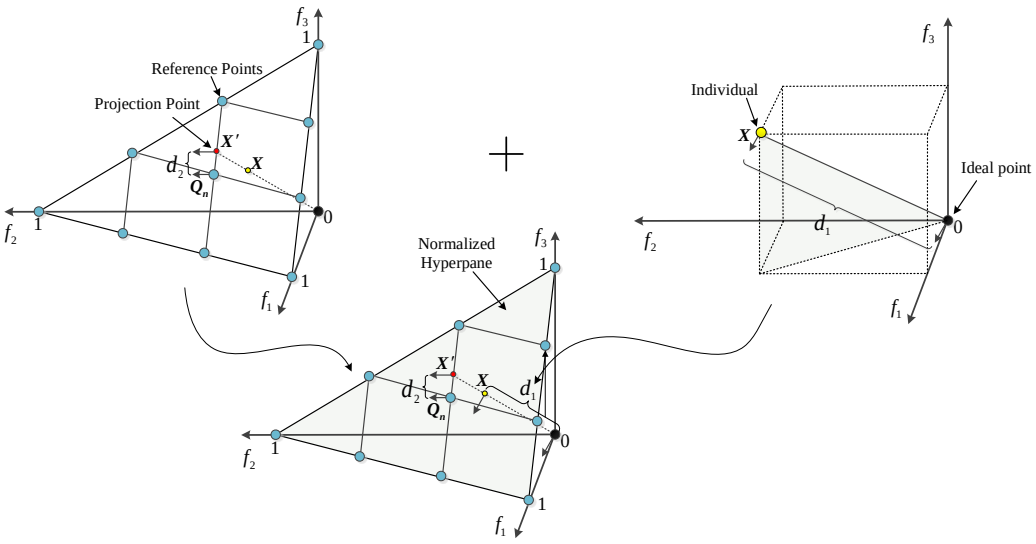

Fig. 3 Solution projection in a normalized hyperplane for a three-objective problem.

Fig.4 illustrates the flowchart of the proposed multi-level management strategy with EMOHT. In each time slot, the local optimization model in (9)-(25) is executed by MG-EMS. Based on the local optimization results, MG-EMS will provide its surplus, shortage and increasable amounts of electricity and gas to the CEMS. After gathering all the information from the lower level, CEMS will run the global optimization model in (26)-(40), and the scheduling decisions will be sent to the middle level. Then, EMOHT is utilized in the middle level to solve the many-criteria optimality model in (41)-(57), and the many-objective Pareto front solutions can be obtained by using (58)-(61). Subsequently, to obtain the optimum solution among the resulting Pareto front solutions by using the hyperplane projection mechanism, the solution whose

projected point is nearest to the centroid of hyperplane is selected as the energy scheduling decision.

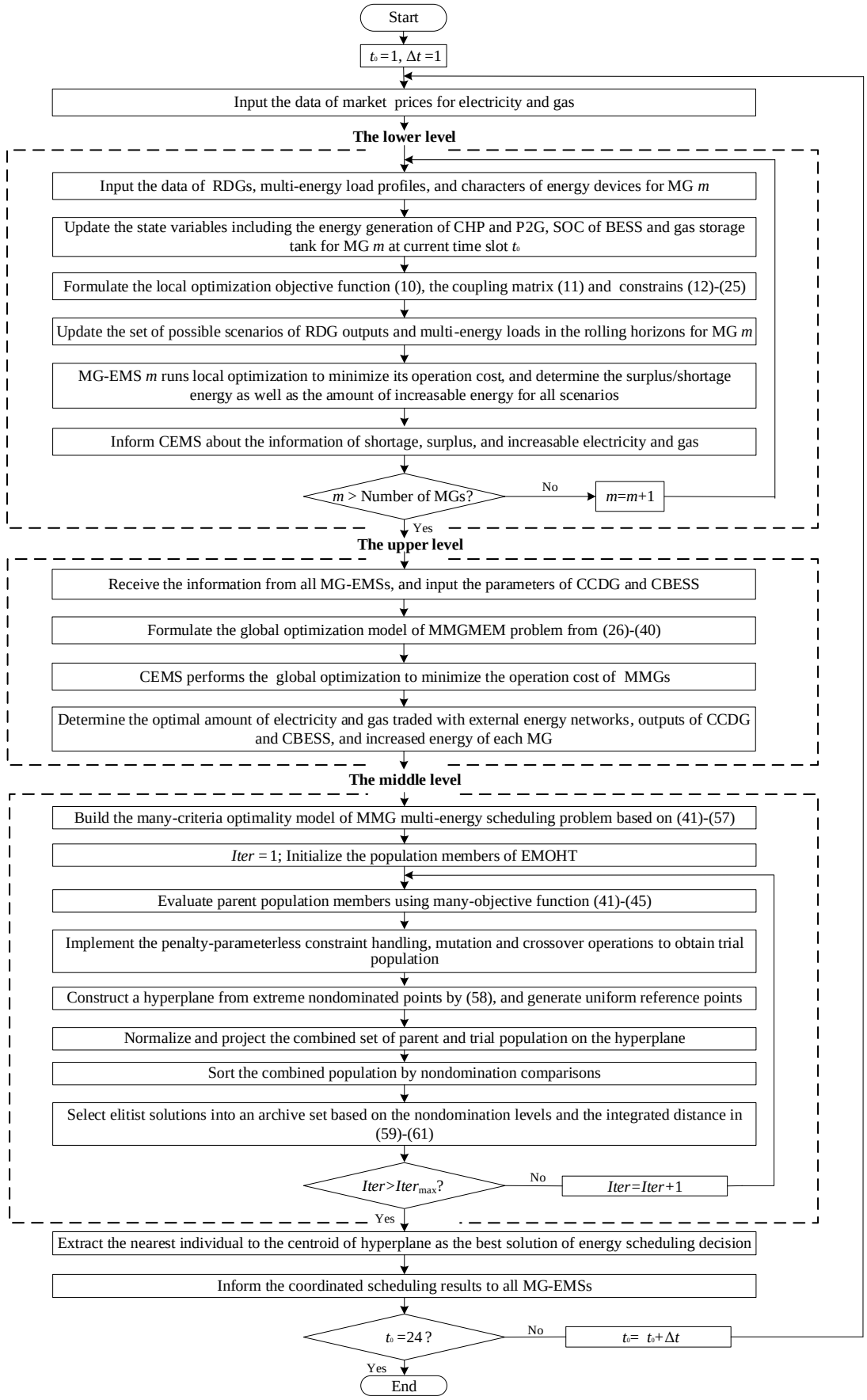

Fig 4 Flowchart of the proposed tri-level MMG multi-energy management strategy with EMOHT.

4 Case Studies

4.1 System Data

The proposed multi-energy management strategy is tested on a MMG system consisting of six interconnected MGs to corroborate its effectiveness. The detailed characteristics of system devices are given in Table 1, which are taken from Bui et al. (2016) and Yang et al. (2021). In this study, heterogeneous MGs are equipped with different quantities and capacities of multi-energy devices and have diverse load characters, resulting in different willingness for multi-energy exchange among MMGs, and the model parameter settings of energy devices in these MGs are listed in Table 2. The power price of electrical utility is derived from Arefifar et al. (2017), and the gas price is set at 0.5 \$/m^3. The feed-in prices of power and gas are set as 0.01 \$/kWh and 0.25 \$/m^3 (Xu et al., 2020), and the unit prices of power and gas exchange among MGs are set to 0.031 \$/kWh and 0.4 \$/m^3, respectively (Jadhav et al., 2019). Furthermore, the rolling horizon optimization of MMG multi-energy scheduling is implemented. The control horizon is 1 hour, and the prediction horizon T is set as 24 hours. The predicted daily load profiles and renewable outputs are adopted from the historical data in (Yang et al., 2019) and (Xu et al., 2020), and their forecasting errors are assumed to follow Gaussian probability distributions. Then, a Monte Carlo sampling approach is utilized to form the initial scenario tree with 2000 scenarios for capturing forecasting uncertainties, and the occurrence probability of each scenario is 1/2000. To decrease the computational cost, a scenario reduction technique in (Heitsch and Romisch, 2003) is further adopted, and only 20 scenarios that have a satisfactory approximation of uncertainties are retained for MMG multi-energy management.

The EMOHT algorithm is compared with state-of-the-art evolutionary many-objective optimization (EMO) algorithms including non-dominated sorting genetic algorithm II (NSGA-II) (Deb et al., 2002), multi-objective evolutionary algorithm based on decomposition (MOEA/D) (Zhang and Li, 2007), NSGA-III (Deb and Jain, 2014), and MOEA/D with a two-phase strategy and a niche-guided scheme (MOEA/D-TPN) (Jiang et al., 2016). These algorithms have been extensively utilized to solve multi-objective optimization or many-objective optimization problems with excellent performance in convergence and solution searching. For each algorithm, 50 independent runs are executed to obtain fifty different optimum solutions by using the concept of solution pools in (Wichmann, 2019). Then, fifty sets of non-dominated solutions are combined and ranked by the dominance comparisons, and the top-ranked solution is selected to further compare and analyze. The settings of parameters have been heuristically well-tuned according to numerous benchmarked tests and simulations. For a fair comparison of results of all algorithms, the maximum iteration and population size are the same and are set to 500 and 200, respectively. Besides, the crossover probability is set as 0.9, and the mutation probability of $1/n$ is used, which is inversely related to the number of decision variables (Deb et al., 2002). Also, the number of reference points is set to 200.

Table 1 Characteristics of energy devices in the MMG system.

CCDG	a=0.00111	b=0.462	c=25
	$P^{\mathrm{CCDG,min}}$=0	$P^{\mathrm{CCDG,max}}$=600 kW	$R^{\mathrm{CCDG,up}} = R^{\mathrm{CCDG,down}}$=200 kW/h
CBESS	$SOC_{\min}$=0.1	$SOC_{\max}$=0.9	$P_{m,t}^{\mathrm{CBESS,ch}}$=$P_{m,t}^{\mathrm{CBESS,dis}}$=80 kW
	$E^{\mathrm{CBESS,R}}$=500 kWh	μ^{CBESS}=0.01 $/kWh	η^{ch}=η^{dis} =0.95
Line Capacity	$P_{\max}^{\mathrm{line}}$ =2000 kW	$V_{\max}^{\mathrm{pipeline}}$ =200 m^3	

Table 2 Characteristics of six MGs in the studied MMG system.

CHP	$P_m^{\mathrm{CHP,max}}$=[250, 200, 300, 350, 180, 280] kW	$P_m^{\mathrm{CHP,min}}$ =[0, 0, 0, 0, 0, 0] kW
	$\eta_m^{\mathrm{CHP,H}}$=[0.44, 0.45, 0.43, 0.45, 0.45]	$\eta_m^{\mathrm{CHP,E}}$ =[0.41, 0.39, 0.4, 0.41, 0.4]
BESS	μ_m^{BESS}=[0.01, 0.01, 0.01, 0.01, 0.01, 0.01] $/kWh	η_m^{ch} =[0.97, 0.95, 0.93, 0.91, 0.94, 0.9]
	$E_{m,i}^{R}$ =[330, 400, 350, 420, 380, 200] kWh	η_m^{dis} =[0.91, 0.95, 0.93, 0.91, 0.94, 0.9]
	$SOC_{m,i}^{\mathrm{BESS,min}}$=[0.1, 0.1, 0.1, 0.1, 0.1, 0.1]	$SOC_{m,i}^{\mathrm{BESS,max}}$=[0.9, 0.9, 0.9, 0.9, 0.9, 0.9]
	$P_m^{\mathrm{BESS,ch}}$=[96, 110, 80, 70, 90, 100] kW	$P_m^{\mathrm{BESS,dis}}$=[85, 100, 80, 90, 95, 115] kW
Gas Tank	$V_m^{\mathrm{Tank,ch,max}}$=[55, 60, 70, 65, 55, 80] m^3/h	$SOC_m^{\mathrm{Tank,min}}$=[0, 0, 0, 0, 0, 0]
	$V_m^{\mathrm{Tank,dis,max}}$=[55, 60, 70, 65, 55, 80] m^3/h	$SOC_m^{\mathrm{Tank,max}}$=[1, 1, 1, 1, 1, 1]
	V_m^{R}=[80, 90, 85, 70, 75, 90] m^3	
Boiler	$Q_m^{\mathrm{Boi,max}}$=[220, 300, 400, 350, 490, 390] kW	η_m^{Boi}=[0.79, 0.78, 0.75, 0.7, 0.7, 0.77]
Furnace	$Q_m^{\mathrm{Fur,max}}$ =[280, 290, 330, 410, 425, 470] kW	η_m^{Fur}=[0.78, 0.75, 0.7, 0.8, 0.75, 0.77]
P2G	$V_m^{\mathrm{P2G,max}}$ =[87, 80, 55, 85, 70, 90] m^3	η_m^{P2G}=[0.63, 0.6, 0.61, 0.62, 0.58, 0.63]

4.2 Scheduling results of MMGs

In the lower level, each MG-EMS optimally schedules its components to determine the surplus/ shortage amount of electricity and gas for each MG. Fig. 5 illustrates the surplus/shortage energy of MMGs, where a positive value denotes a shortage of energy, and a negative value means energy is surplus. It is observed in Fig. 5 that MG3 and MG4 have surplus energy, while other MGs suffer from an energy shortage. Then, MG-EMSs inform their surplus/shortage amount of energy to C-EMS in the upper level. The outputs of system devices are determined by the C-EMS, as shown in Fig. 6. It can be found from Fig. 6 that, to minimize the total operation cost and maintain the MMG energy balance, CBESS charges in off-peak hours and discharges during peak hours. CCDG operates at peak hours to meet MMG energy demands.

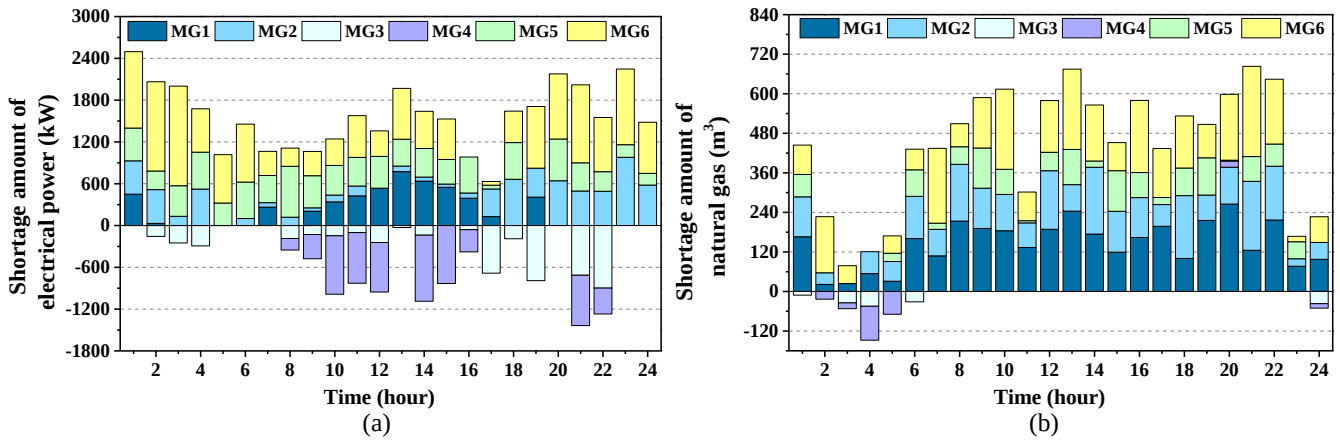

Fig. 5 Shortage and surplus amounts of energy for each MG a) electrical power, b) natural gas.

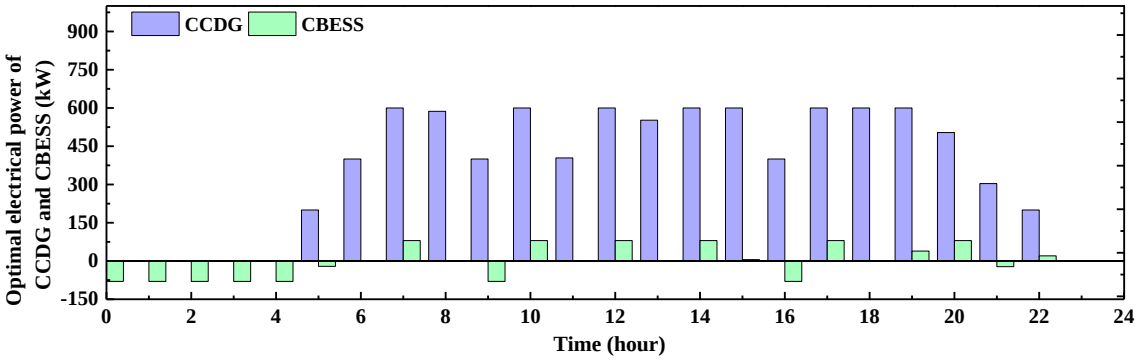

Fig. 6 The output power of CCDG and CBESS.

In the middle level, based on the optimized results from the upper level, the many-criteria optimality model is implemented to coordinate the multi-energy sharing among MMGs. The electricity and gas balance of MG1 and MG4 are illustrated in Fig. 7. It can be found that MG1 with a shortage of energy not only buys electricity and gas from energy networks but also actively receives energy from other adjacent MGs. In MG4, the surplus electricity from PVs and WTs is shared with other MGs for relieving their load burden during hours 8-22. Because the electrical loads are low and renewable outputs are relatively high during hours 2-5, MG4 converts surplus power into synthetic natural gas by P2G and then transmits these gas products to other MGs. Besides, MGs with feasible capacities, such as MG4, can increase their electrical and gas production and then share energy resources with other MGs to obtain the corresponding incomes.

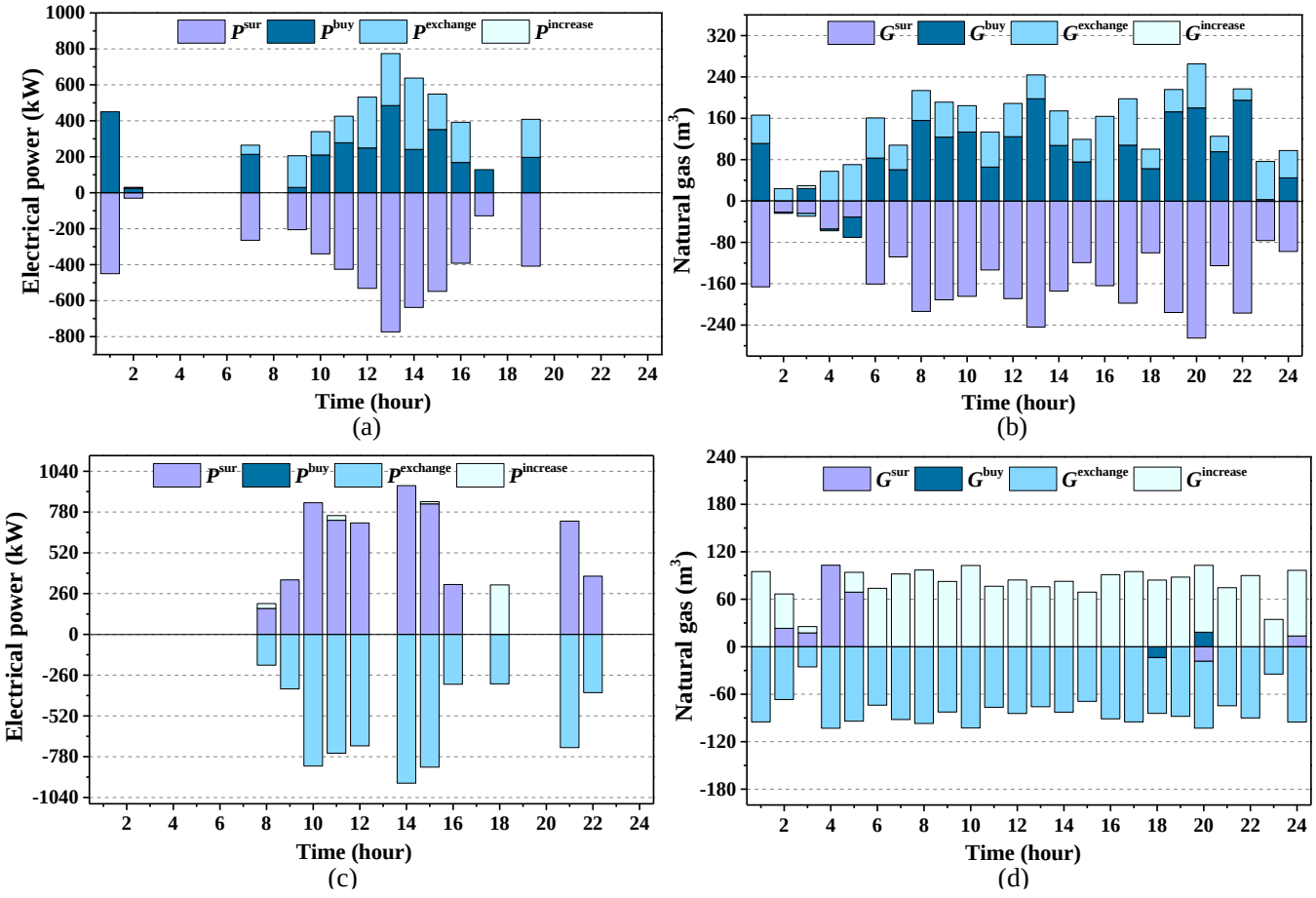

Fig. 7 Electrical power and gas distribution situation of MG1 and MG4 a),b) MG1, c),d) MG4.

Fig. 8 shows the internal power and gas interaction within MMGs. It can be found from Fig. 8(a) that all MGs interactively exchange energy sources with each other. During hours 7-22, MG3 and MG4 have relatively higher renewable outputs than other MGs, and then sell their surplus electricity to other MGs with energy demand. From Fig. 8(b), the shortage of gas for MG1 and MG2 is fulfilled by energy sharing, while MG3 and MG4 send their redundant gas to other MG with gas needs. MG 5 and MG6 can switch their role based on their amount of surplus or shortage gas. For instance, MG5 participates in gas sharing as a sender during hours 2 and as a receiver during hours 6-22. It is observed in Fig. 8 that the sum of exchanged energy is equal to zero, which validates that the supply-demand balance constraints (48) and (49) are well satisfied. Fig. 9 presents the amount of increasable energy for MMGs. It can be observed that the total amount of increasable energy can be impartially allocated to MGs with feasible capacities.

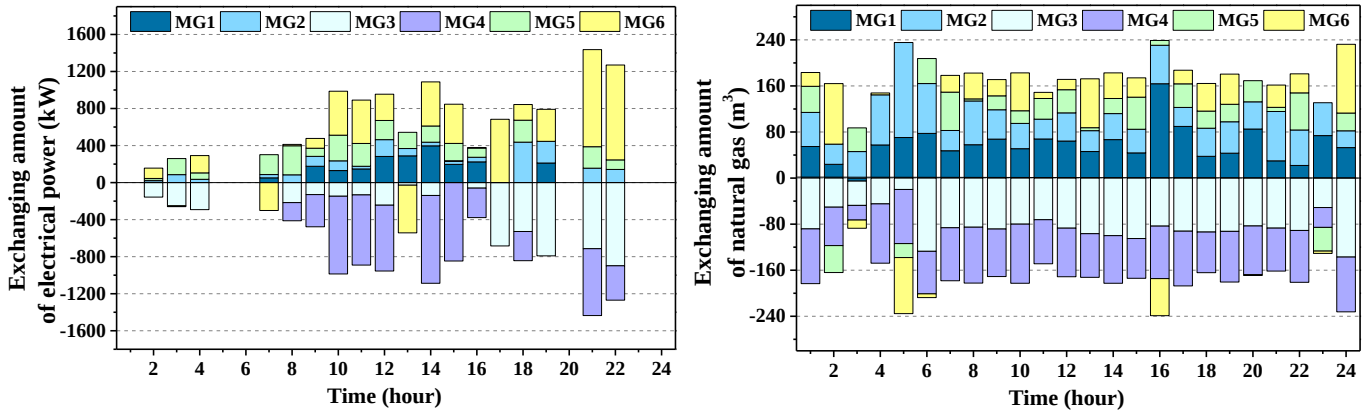

(a) (b)

Fig. 8 Scheduling results of multi-energy exchanges among MGs a) electrical power, b) natural gas.

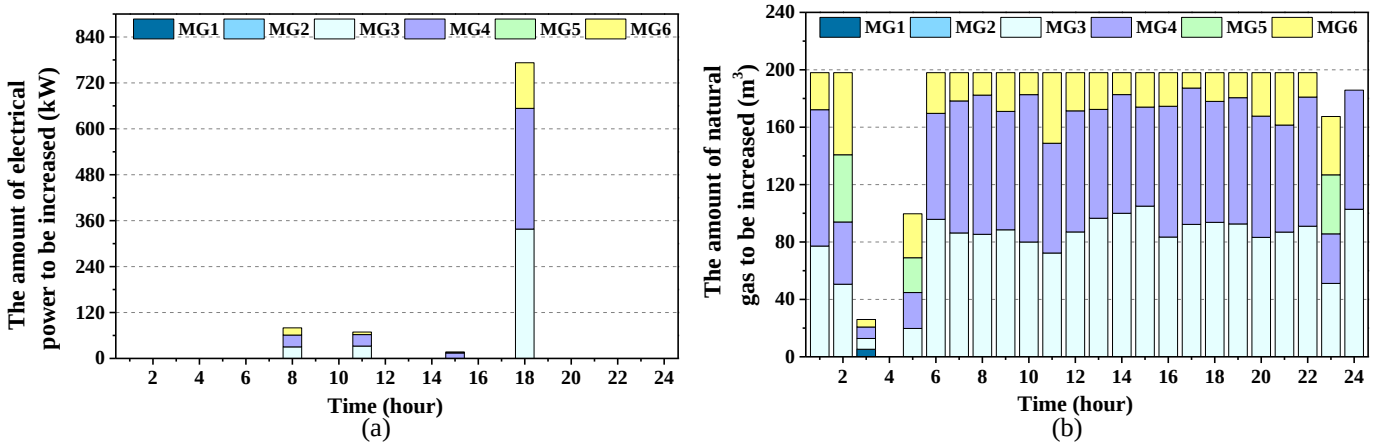

(a) (b)

Fig. 9 Scheduling results of increasable energy for each MG a) electrical power, b) natural gas.

4.3 Comparative Results

The multi-energy management strategy proposed in this paper was compared with the other three strategies. The details of all the strategies are listed in Table 3. Strategy 1 is the proposed strategy established in Section 3. Strategy 2 is a centralized strategy in (Wang et al., 2018), where a single-objective model is developed to manage the multi-energy supply and demand of MMGs. Strategy 3 is a hierarchical

energy management strategy in (Bui et al., 2016) where multi-energy interactions are ignored. Strategy 4 is the no-coordinated strategy in which each MG only focuses on its objective without considering multi-energy couplings and interactions. In this paper, strategy 4 is defined as the basic strategy for comparison.

Table 3 Characteristics of strategies 1-4 in the comparative study.

Strategy	Type	Technological details (objective function=operation cost)
1	Proposed	Considering the multi-energy couplings and interactions, and a tradeoff of MMG benefits
2	Centralized	Optimizing the MMG multi-energy couplings and interactions by a single-objective model
3	Hierarchical	No gas exchanging among MMGs
4	No-coordinated	No multi-energy couplings and interactions

Table 4 tabulates the best solution for operation cost obtained by the best optimization run of the proposed strategy, as well as the optimized results of other strategies, where the negative value of cost denotes a profit. It can be found from Table 4, compared with basic strategy 4, the proposed strategy can achieve a cost saving for all MGs with different energy devices and willingness of energy sharing. For example, MGs under energy shortage, such as MG1, MG2, MG5, and MG6, can save 21.54%, 19.07%, 22.55% and 24.15% of operation cost, respectively, and MGs with surplus energy can also receive a profit increment. Thus, with the proposed strategy, an optimum and coordinated condition for MMGs is achieved because all MGs can benefit from the multi-energy sharing. For the centralized strategy 2, MGs with surplus energy and residual capacities, such as MG 3 and MG4, can receive benefits for the energy exchange compared with strategy 4, as shown in Table 4. However, about a third of MGs, such as MG5 and MG6, incur losses from energy exchange with other MGs, while MG 1 and MG 2 gain most of the benefits. In this case, if a centralized strategy is adopted to achieve a minimal operation cost of MMGs, the benefits of some MGs in the MMG system may be damaged, seriously reducing the enthusiasm of multi-energy sharing among MMGs. Besides, it can be found from Table 4 that, the energy trading between MGs and energy networks will significantly increase if the gas exchange among MGs is not considered, and thus the cost of each MG in strategy 3 is much higher than strategies 1 and 2.

Fig. 10 illustrates the comparison results of the system net load curve for four comparative strategies. It is observed in Fig. 10 that, MMGs in strategy 1 sell their surplus energy to the electrical network during hours 2-5, while the surplus electricity of MMGs in strategy 1 is not sold to the electrical network. This is mainly because surplus renewable sources can be shared among MGs in strategy 1rather than feeding back to the electrical grid. Furthermore, the surplus power can be converted to gas by P2G during valley periods in strategy 1, and the surplus gas can be shared among MGs. Thus, with the proposed strategy, the peak demand of both electricity and gas in MMGs can be effectively mitigated. The system performance results on the renewable accommodation and system operation cost obtained with strategies 1-4 have been further compared, as shown in Table 5. It can be found from Table 5 that, compared with strategy 3, the system

operation cost and the renewable accommodation in strategy 1 are reduced by 14.8% and increased by 1.4%, respectively. Besides, compared with strategy 4, the system operation cost in strategy 1 is reduced by 33.2%, and the renewable accommodation is up by 12.2%. Moreover, the comparative studies of the proposed and centralized strategy on average computational time are listed in Table 6. It can be found from Table 5 and Table 6 that, gaps of system operation cost between the proposed strategy and the centralized strategy are less than 0.2%, while the running time of the proposed strategy is significantly reduced, especially for the large scale MMGMEM problems. The simulation results indicate the proposed strategy shows the most competitive overall performance on optimized results and computational time compared with other strategies, and it can well satisfy the real-time applicability and requirement of MMGMEM problems.

Table 4 Comparative cost results of six MGs with strategies 1-4.

Index of MGs	Related to energy networks		Related to other MGs		Operation cost of devices($)	Individual cost ($)	Cost saving ($)
	Electricity buying cost ($)	Gas buying cost ($)	Electricity buying cost ($)	Gas buying cost ($)			
Strategy 1: Proposed strategy							
MG 1	241.30	1,039.20	65.42	556.01	37.37	1,939.30	532.49
MG 2	283.65	597.07	57.53	549.81	36.00	1,524.06	359.13
MG 3	-0.40	0.000	-167.58	-794.08	515.27	-446.79	554.38
MG 4	0.00	2.35	-197.58	-777.67	490.46	-482.44	681.20
MG 5	431.36	293.87	87.40	218.38	65.18	1,096.19	319.07
MG 6	529.99	1,040.38	154.81	247.56	182.22	2,154.96	686.12
Strategy 2: Centralized strategy							
MG 1	113.19	772.70	107.27	408.97	37.52	1,439.65	1,032.14
MG 2	195.06	78.78	96.38	724.44	36.00	1,130.66	752.53
MG 3	-0.11	0.00	-183.66	-796.60	448.58	-531.79	639.37
MG 4	0.00	-8.26	-194.45	-819.01	371.74	-649.98	848.74
MG 5	267.93	238.02	147.63	505.24	319.35	1,478.17	-62.91
MG 6	909.83	1,891.63	26.83	-23.03	105.90	2,911.16	-70.08
Strategy 3: Hierarchical strategy							
MG 1	243.17	1,736.84	16.39	0.00	65.35	2,061.75	410.04
MG 2	286.59	1,284.33	17.44	0.00	61.78	1,650.14	233.05
MG 3	-0.32	-79.41	-155.19	0.00	48.00	-186.92	294.50
MG 4	0.00	-104.04	-186.20	0.00	48.26	-241.98	440.74
MG 5	432.58	622.97	67.39	0.00	54.70	1,177.64	237.62
MG 6	523.88	1,627.92	240.17	0.00	20.23	2,412.20	428.88
Strategy 4: No-coordinated strategy (basic strategy)							
MG 1	809.10	1,614.56	0.00	0.00	48.13	2,471.79	0.00
MG 2	727.75	1,103.94	0.00	0.00	51.50	1,883.19	0.00
MG 3	-196.10	257.29	0.00	0.00	46.39	107.58	0.00
MG 4	-409.72	556.24	0.00	0.00	52.24	198.76	0.00
MG 5	904.73	482.26	0.00	0.00	28.27	1,415.26	0.00
MG 6	1,509.14	1,294.63	0.00	0.00	37.31	2,841.08	0.00

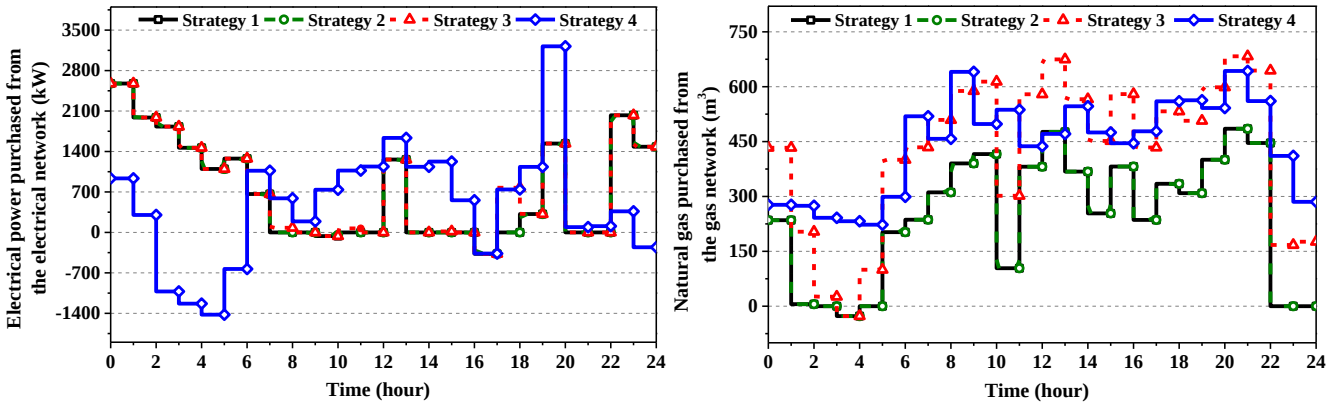

Fig. 10 System net load profiles optimized with different strategies a) electrical power, b) natural gas.

Table 5 Comparative system performance results of different strategies.

Strategy	1	2	3	4
CBESS degradation cost ($)	11.48	16.27	10.13	22.27
CCDG generation cost ($)	437.52	434.69	433.27	395.13
Renewable accommodation (%)	99.48	99.50	98.12	88.66
System operation cost ($)	6,234.28	6,228.83	7,316.23	9,335.06

Table 6 Comparisons of the average running time between proposed and centralized strategy.

Number of MGs	Running time (min)	
	Proposed strategy 1	Centralized strategy 2
6	3.63	4.92
50	14.61	18.42
100	26.10	32.75
200	36.51	53.62
400	53.46	89.48

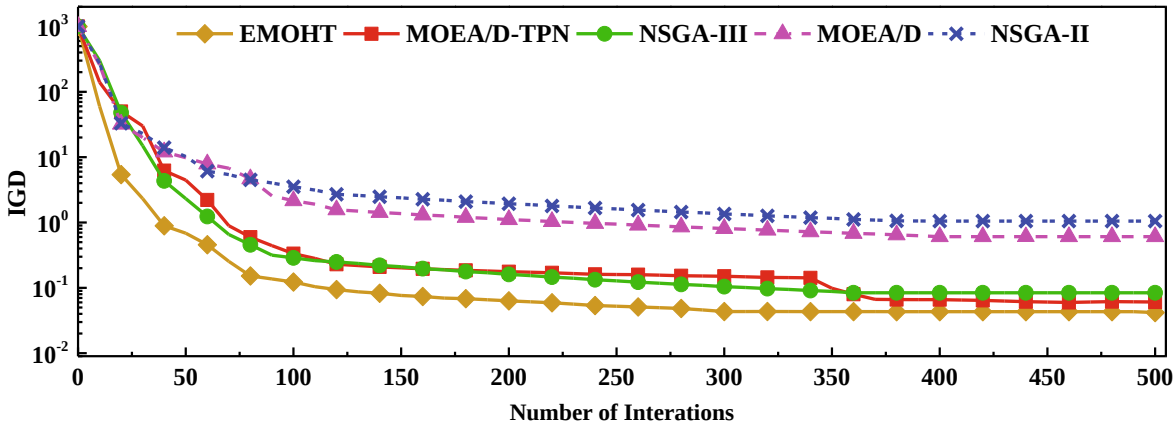

Fig. 11 Variation of the mean IGD value in the convergence process.

Table 7 Average computational time of the MMGMEM with different algorithms

	EMOHT	MOEA/D-TPN	NSGA-III	MOEA/D	NSGA-II
Run time (min)	3.63	5.15	5.53	7.52	12.47

Furthermore, to demonstrate the superior performance of the EMOHT algorithm, four other advanced EMO algorithms, including NSGA-II (Deb et al., 2002), MOEA/D (Zhang and Li, 2007), NSGA-III (Deb

and Jain, 2014), and MOEA/D-TPN (Jiang et al., 2016), were used to solve the MMGMEM problem, and further compared with the EMOHT. For comparisons, the inverse generational distance (IGD) in (Jiang and Yang, 2016) is adopted for measuring the solution quality on the diversity and convergence of non-dominated solutions from different algorithms, and the smaller value of IGD represents a better performance of the algorithm. All the simulations were performed in MATLAB 2014a platform and ran on a personal computer with a 4-GHz Intel Core i7 CPU and 64 GB RAM. The results over the mean IGD metric and the average run time of MMGMEM with different algorithms are shown in Fig. 11 and Table 7, respectively. It can be found that EMOHT markedly outperforms other algorithms, and provides satisfactory performance on various measures.

In order to demonstrate the solution quality of the proposed strategy, 50 different solutions obtained from 50 independent runs of the proposed strategy were compared with the optimal solution of the centralized strategy. Specifically, the solution of the centralized strategy was compared with the best solution (top-ranked solution), the worst solution (last-ranked solution), and the mean solution of the proposed strategy, and comparative results are listed in Table 8. It can be found from Table 8 that the best, worst, and mean solutions of the proposed strategy are all better than the solution of the centralized strategy because all MGs achieve a cost saving and none of them suffer a loss. Moreover, the robustness performance of the EMOHT algorithm was tested. The statistical analysis was performed for the optimization results of different algorithms over 50 runs, as shown in Table 9. Four typical statistical parameters, including the minimum value, maximum value, average value and standard deviation, were used to compare and analyze the solution performance. The resulting statistics show that, compared with other algorithms, results obtained by EMOHT algorithm have a lower standard deviation, and the difference between the minimum and maximum operation cost of each MG is the lowest among all algorithms. Meanwhile, simulations also prove that the average solution of 50 runs obtained by EMOHT is better than the average solution obtained by other algorithms. The resulting statistics demonstrate that EMOHT can effectively provide satisfactory solutions for each optimization run, and verify its high degree of robustness.

Table 8 Comparative analyses of optimized cost obtained from the proposed and centralized strategies.

Index of MGs	Centralized strategy		Proposed strategy							
			Best solution		Worst solution		Mean solution		Standard deviation	
	Operation cost ($)	Cost saving ($)	Operation cost ($)	Cost saving ($)	Operation cost ($)	Cost saving ($)	Operation cost ($)	Cost saving ($)	Operation cost	Cost saving
MG 1	1,439.65	1,032.13	1,939.30	532.48	1,946.59	525.20	1,946.11	525.68	6.52	6.52
MG 2	1,130.66	752.54	1,524.06	359.14	1,540.64	342.55	1,530.42	352.77	5.67	5.67
MG 3	-531.79	639.37	-446.79	554.38	-455.75	563.33	-449.21	556.79	6.92	6.92
MG 4	-649.98	848.74	-482.44	681.20	-491.88	690.64	-485.28	684.04	4.47	4.47
MG 5	1,478.17	-62.91	1,096.19	319.07	1,107.57	307.70	1,098.46	316.8	5.06	5.06
MG 6	2,911.16	-70.07	2,154.96	686.12	2,138.12	702.97	2,144.77	696.31	9.88	9.88

Table 9 Resulting statistics of operation cost of MGs in 50 independent runs

Algorithm	MG1				MG2				MG3			
	Min.	Max.	Average	Std. dev.	Min.	Max.	Average	Std. dev.	Min.	Max.	Average	Std. dev.
EMOHT	1,939.30	1,956.62	1,946.11	6.52	1,523.81	1,540.64	1,530.42	5.67	-463.76	-441.30	-449.21	6.92
MOEA/D-TPN	1,949.34	2,011.23	1,984.40	17.86	1,539.33	1,590.44	1,564.55	14.93	-453.03	-413.58	-428.29	11.41
NSGA-III	1,952.46	1,997.93	1,987.34	15.62	1,537.34	1,573.81	1,558.25	11.67	-440.03	-417.87	-419.88	14.41
MOEA/D	2,014.47	2,691.45	2,225.17	225.94	1,621.39	2,173.38	1,787.66	179.64	-398.63	-274.98	-335.75	31.47
NSGA-II	2,042.45	3,606.54	2,573.17	505.85	1,637.60	2,912.33	2,073.30	399.61	-382.32	-238.37	-302.04	39.92
	MG4				MG5				MG6			
	Min.	Max.	Average	Std. dev.	Min.	Max.	Average	Std. dev.	Min.	Max.	Average	Std. dev.
EMOHT	-491.88	-479.01	-485.28	4.47	1,091.27	1,107.56	1,098.46	5.06	2,128.88	2,154.96	2,144.77	9.88
MOEA/D-TPN	-483.21	-456.31	-474.53	5.63	1,119.26	1,154.75	1,134.68	10.39	2,144.52	2,201.36	2,180.59	16.43
NSGA-III	-479.80	-441.91	-467.34	10.17	1,135.05	1,163.80	1,147.48	12.22	2,164.49	2,208.76	2,190.22	14.25
MOEA/D	-456.18	-398.47	-410.70	21.38	1,175.85	1,591.17	1,321.62	128.13	2,236.50	3,060.24	2,470.24	249.73
NSGA-II	-425.63	-250.61	-368.06	59.00	1,187.61	2,132.16	1,574.19	314.27	2,258.86	4,100.72	2,855.21	599.67

4.4 Discussion

In this subsection, a sensitivity analysis was conducted to evaluate the impact of the number of MGs on the performance of the proposed strategy. The number of MGs was assumed to be 6, 30, 50, 100, 200, 300 and 400, respectively. The model parameter settings of multi-energy devices, load profiles as well as outputs of renewable energy in these MGs were randomly obtained within certain ranges on the statistical data from previous works in Section 4.1. Simulation results of the total operation cost of MMGs under various numbers of MGs are illustrated in Fig. 12. It can be found that, the system operation cost remarkably increases with the increased number of MGs. In addition, in the case of six MGs, the comparative studies were performed with various lengths of the prediction and control horizon associated with rolling horizon procedures, and a perfect prediction over a week (168 hours) is assumed as a base case. The results of system operation cost and renewable energy accommodation under different lengths of predicted and controlled horizon are shown in Table 10 and Table 11, respectively. It can be found from Table 10 that, compared with the based case (168 hours), under the case of 1-h control horizon, the rolling horizon procedures slightly increase the system operation cost by 0.03% at 24 h and 0.007% at 96 h, while the renewable accommodation is reduced by 0.16% at 24h and 0.06% at 96 h. Although the prediction accuracy decreases when the length of the prediction horizon increases, increasing the length of the prediction horizon in short-term forecasting can improve the optimized results because more future information of MMGs is considered. Thus, for the 1-h length of control horizon, the system operation cost slightly decreases as the length of the prediction horizon increases from 6 h to 96 h, while the renewable accommodation is slightly increased. As the length of the prediction horizon continues to increase, the improvement rates of optimized results decrease. For example, the gap of system operation cost between the 24-h and 96-h prediction horizon is close to 0.1%. However, a longer prediction horizon indicates that more data and longer processing time are required (Langer and Volling, 2020). It can be found from Table 11 that, under the same length of prediction horizon, the system operation cost rises with the increased

length of control horizon, while the renewable accommodation is decreased. It is worth noting that, for the 24-h prediction horizon, a large gap occurs between the optimized results of the 12-h and 24-h control horizon, and optimized results are improved with the reduction of the control horizon. The simulation results further confirm the end-of-horizon effects mentioned in (Langer and Volling, 2020).

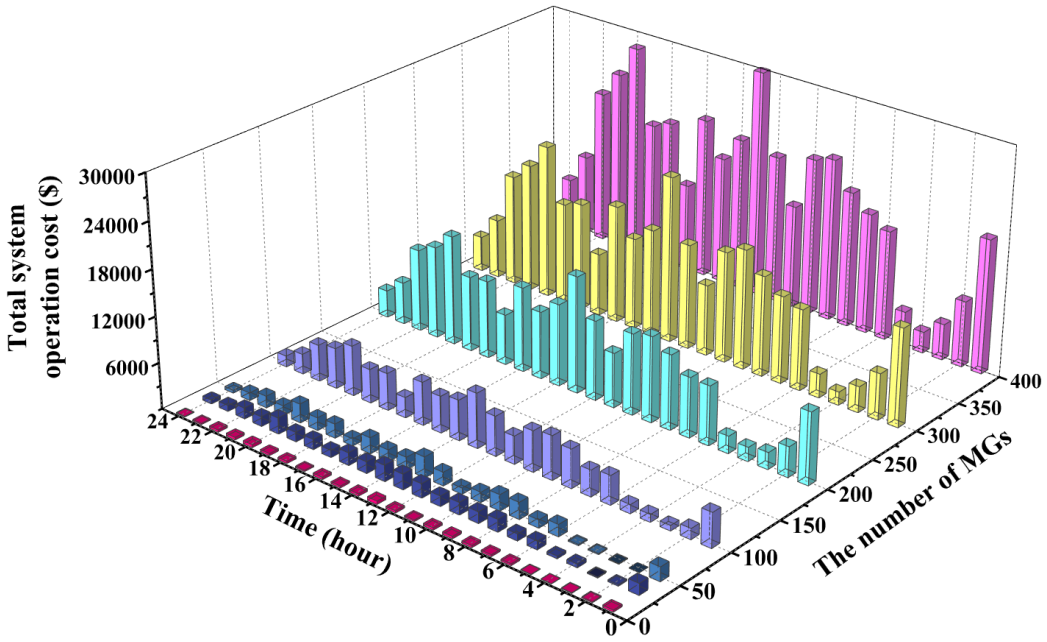

Fig. 12 System operation cost versus different number of MGs with the proposed strategy

Table 10 The optimized results of the rolling horizon procedure under different prediction horizons

Prediction horizon (hour)	168	6	12	24	36	48	72	96
Control horizon (hour)	168				1			
System operation cost ($)	43,538.24	43,571.67	43,557.32	43,551.91	43,548.42	43,545.39	43,543.53	43,541.47
Renewable accommodation (%)	99.69	98.93	99.41	99.53	99.57	99.58	99.61	99.63

Table 11 The optimized results of the rolling horizon procedure under different control horizons

Prediction horizon (hour)	168	24			48			96		
Control horizon (hour)	168	6	12	24	6	12	24	6	12	24
System operation cost ($)	43,538.24	43,554.34	43,558.31	43,751.52	43,547.31	43,549.91	43,554.27	43,541.67	43,542.32	43,544.59
Renewable accommodation (%)	99.69	99.48	99.34	78.61	99.57	99.56	99.46	99.63	99.62	99.60

Here, the practical applicability of the proposed strategy is further briefly discussed. In a practical MMG system, uncertainties of energy outputs from RDGs and multi-energy loads are not fixed due to the time-varying weather condition and energy consumption behaviors. These uncertainties have brought unprecedented difficulties and challenges for maintaining the supply-demand balance and making energy management decisions. To tackle uncertainties in MMG operation, a scenario-based stochastic scheduling with the rolling procedure is introduced into the proposed strategy, as aforementioned in Section 3. Besides, in the proposed strategy, only a limited amount of information, such as surplus or shortage energy of each MG, is shared, and thus the information privacy can be well preserved. Furthermore, assumptions taken in

Section 3.1 are also reasonable under normal operating conditions of MMGs. These assumptions have been widely made in previous works, such as in (Cui et al., 2016). Hence, the introduction of the above assumptions will not hinder the practicability and reliability of the proposed strategy. Therefore, the proposed strategy can be well used in current EMS platforms for industrial, residential, and other types of MMGs to assist their operators with decision making and facilitate the coordinated operation of MMGs.

5 Conclusions

In this paper, the multi-energy coupling and interactions within MMGs are modeled as a MMG multi-energy coupling matrix, which is further reformulated into the sum of three linear and sparse submatrices by the developed multi-step matrix decomposition technique. Then, an interactive tri-level multi-energy management strategy is proposed to solve the optimum MMGMEM problem based on many-criteria optimality. The MMG multi-energy scheduling problem is decomposed into reduced-complexity tri-level optimization sub-problems. The effectiveness and scalability of the proposed strategy have been fully tested on MMG systems with numerous heterogeneous MGs. The key findings are summarized as follows:

1) By leveraging the interactions of multiple levels to coordinate the multi-energy management of the MMG system, the proposed strategy can outperform other MMG energy management strategies on system operational economy and local renewable accommodation, with a decrease in overall MMG operation cost by over 14.8% and an increase on renewable energy utilization by over 1.5%. Also, the system net load characters of electricity and gas in MMGs can be effectively improved.

2) The many-criteria optimality model can fully exploit the flexibility of multi-energy conversion and interaction to coordinate the multi-energy sharing among multiple heterogeneous MGs. Thus, the MMG multi-energy sharing problem can obtain an optimum tradeoff in which all MGs can benefit from electricity-gas exchanges, saving more than 19% of operation cost for each MG than uncoordinated strategy.

3) The average computational time of the proposed strategy is shortened significantly compared with the centralized strategy for MMGMEM problems. Especially for the large scale MMGs such as hundreds of MGs, the computational time is even reduced by more than 30%. The time performance further validates the superior scalability of the strategy in solving the optimum multi-energy management problem with numerous heterogeneous MGs.

In MMGs, the number of MGs participating in multi-energy sharing and trading may increase dramatically, which will bring serious challenges to the MMG communication in respect of timeliness, scalability, coverage, and transmission rate. Thus, in our future work, efforts will be made to incorporate the impact assessment of communication reliability (such as communication delays and limited bandwidth) into the proposed strategy for improving its applicability in MMGMEM problems.

Acknowledgment

This work was jointly supported by the Research Grants Council of the HKSAR Government (Grant No. R5020-18), the Innovation and Technology Commission of the HKSAR Government to the Hong Kong Branch of National Rail Transit Electrification and Automation Engineering Technology Research Center (Grant No. K-BBY1), the National Natural Science Foundation of China (51877072), and the State Key Laboratory of Alternate Electrical Power System with Renewable Energy Sources (No. LAPSS20005).

Appendix A

At the third step of the developed multi-step matrix decomposition technique in Section 2.3, (A.1) is nonlinear due to the introduction of dispatch factors. In this paper, state variables are used to avoid introducing dispatch factors, and the detailed derivation process is provided as below.

$$\underbrace{\begin{bmatrix} L_m^{\mathrm{E}} \\ L_m^{\mathrm{H}} \\ L_m^{\mathrm{Gas}} \end{bmatrix}}_{\boldsymbol{L}_m} = \underbrace{\begin{bmatrix} f^{\mathrm{WT}} v_m^{\mathrm{WT,E}} & f^{\mathrm{PV}} v_m^{\mathrm{PV,E}} & v_m^{\mathrm{BESS,E}} & Q^{\mathrm{Gas}} \eta^{\mathrm{CHP,E}} v_m^{\mathrm{Tank,CHP}} v_m^{\mathrm{CHP,E}} \\ f^{\mathrm{WT}} \eta^{\mathrm{Boi}} v_m^{\mathrm{WT,Boi}} v_m^{\mathrm{Boi,H}} & f^{\mathrm{PV}} \eta^{\mathrm{Boi}} v_m^{\mathrm{PV,Boi}} v_m^{\mathrm{Boi,H}} & \eta^{\mathrm{Boi}} v_m^{\mathrm{BESS,Boi}} v_m^{\mathrm{Boi,H}} & Q^{\mathrm{Gas}} (\eta^{\mathrm{CHP,E}} v_m^{\mathrm{Tank,CHP}} v_m^{\mathrm{CHP,Boi}} \eta^{\mathrm{Boi}} + \\ & & & \eta^{\mathrm{CHP,H}} v_m^{\mathrm{Tank,CHP}} + \eta^{\mathrm{Fur}} v_m^{\mathrm{Tank,Fur}}) v_m^{\mathrm{H}} \\ f^{\mathrm{WT}} \eta^{\mathrm{P2G}} v_m^{\mathrm{WT,P2G}} v_m^{\mathrm{P2G,G}} & f^{\mathrm{PV}} \eta^{\mathrm{P2G}} v_m^{\mathrm{PV,P2G}} v_m^{\mathrm{P2G,G}} & \eta^{\mathrm{P2G}} v_m^{\mathrm{BESS,P2G}} v_m^{\mathrm{P2G,G}} & v_m^{\mathrm{Tank,G}} + Q^{\mathrm{Gas}} \eta^{\mathrm{CHP,E}} v_m^{\mathrm{Tank,CHP}} v_m^{\mathrm{CHP,P2G}} \eta^{\mathrm{P2G}} v_m^{\mathrm{P2G,G}} \end{bmatrix}}_{\boldsymbol{M}_{mm}} \underbrace{\begin{bmatrix} W_m^{\mathrm{WT}} \\ G_m^{\mathrm{PV}} \\ P_m^{\mathrm{BESS}} \\ V_m^{\mathrm{Tank}} \end{bmatrix}}_{\boldsymbol{S}_m} \tag{A.1}$$

where values of dispatch factors, such as $v_m^{\mathrm{WT,E}}$, are limited between 0 and 1. Based on energy conversation principles, the following equations must be satisfied.

$$\begin{bmatrix} v_m^{\mathrm{WT,E}} & v_m^{\mathrm{WT,Boi}} & v_m^{\mathrm{WT,P2G}} \\ v_m^{\mathrm{PV,E}} & v_m^{\mathrm{PV,Boi}} & v_m^{\mathrm{PV,P2G}} \\ v_m^{\mathrm{BESS,E}} & v_m^{\mathrm{BESS,Boi}} & v_m^{\mathrm{BESS,P2G}} \\ v_m^{\mathrm{Tank,G}} & v_m^{\mathrm{Tank,Fur}} & v_m^{\mathrm{Tank,CHP}} \end{bmatrix} \begin{bmatrix} 1 \\ 1 \\ 1 \\ 1 \end{bmatrix} = \begin{bmatrix} 1 \\ 1 \\ 1 \\ 1 \end{bmatrix} \tag{A.2}$$

In order to linearize the coupling matrix, the connections and the converter inputs are selected as state variables (Shao et al., 2017). Thus, (A.1) can be described as the following linear equations.

$$L_m^{\mathrm{E}} = P_m^{\mathrm{WT,E}} + P_m^{\mathrm{PV,E}} + P_m^{\mathrm{BESS,E}} + Q^{\mathrm{Gas}} V_m^{\mathrm{Tank,CHP,E,L}} \eta^{\mathrm{CHP,E}} \tag{A.3}$$

$$\begin{aligned} L_m^{\mathrm{H}} = {} & P_m^{\mathrm{WT,Boi}} \eta^{\mathrm{Boi}} + P_m^{\mathrm{PV,Boi}} \eta^{\mathrm{Boi}} + P_m^{\mathrm{BESS,Boi}} \eta^{\mathrm{Boi}} + Q^{\mathrm{Gas}} V_m^{\mathrm{Tank,CHP,E,Boi}} \eta^{\mathrm{CHP,E}} \eta^{\mathrm{Boi}} \\ & + (Q^{\mathrm{Gas}} \eta^{\mathrm{CHP,E}} V_m^{\mathrm{Tank,CHP,E}}) \eta^{\mathrm{CHP,H}} / \eta^{\mathrm{CHP,E}} + Q^{\mathrm{Gas}} V_m^{\mathrm{Tank,Fur}} \eta^{\mathrm{Fur}} \end{aligned} \tag{A.4}$$

$$L_m^{\mathrm{Gas}} = P_m^{\mathrm{WT,P2G}} \eta^{\mathrm{P2G}} + P_m^{\mathrm{PV,P2G}} \eta^{\mathrm{P2G}} + P_m^{\mathrm{BESS,P2G}} \eta^{\mathrm{P2G}} + V_m^{\mathrm{Tank,G}} + Q^{\mathrm{Gas}} V_m^{\mathrm{Tank,CHP,E,P2G}} \eta^{\mathrm{CHP,E}} \eta^{\mathrm{P2G}} \tag{A.5}$$

$$P_m^{\mathrm{WT}} = P_m^{\mathrm{WT,E}} + P_m^{\mathrm{WT,Boi}} + P_m^{\mathrm{WT,P2G}} \tag{A.6}$$

$$P_m^{\mathrm{PV}} = P_m^{\mathrm{PV,E}} + P_m^{\mathrm{PV,Boi}} + P_m^{\mathrm{PV,P2G}} \tag{A.7}$$

$$P_m^{\mathrm{BESS}} = P_m^{\mathrm{BESS,E}} + P_m^{\mathrm{BESS,Boi}} + P_m^{\mathrm{BESS,P2G}} \tag{A.8}$$

$$V_m^{\mathrm{Tank}} = V_m^{\mathrm{Tank,Fur}} + P_m^{\mathrm{Tank,G}} + V_m^{\mathrm{Tank,CHP,E,L}} + V_m^{\mathrm{Tank,CHP,E,Boi}} + V_m^{\mathrm{Tank,CHP,E,P2G}} \tag{A.9}$$

$$V_m^{\mathrm{Tank,CHP}} = V_m^{\mathrm{Tank,CHP,E,L}} + V_m^{\mathrm{Tank,CHP,E,Boi}} + V_m^{\mathrm{Tank,CHP,E,P2G}} \tag{A.10}$$

where $P_m^{\mathrm{WT,E}} = f^{\mathrm{WT}} W_m^{\mathrm{WT}}$, and $P_m^{\mathrm{PV,E}} = f^{\mathrm{PV}} G_m^{\mathrm{PV}}$; $P_m^{\mathrm{WT,E}}$, $P_m^{\mathrm{PV,E}}$ and $P_m^{\mathrm{BESS,E}}$ represent the electricity supplied from WT, PV and BESS to electrical loads, respectively; $V_m^{\mathrm{Tank,CHP,E,L}}$, $V_m^{\mathrm{Tank,CHP,E,Boi}}$ and

$V_m^{\mathrm{Tank,CHP,E,P2G}}$ denote the input amount of gas from the gas tank to CHP, which are used for CHP generation to supply the electrical load, boiler and P2G, respectively. $P_m^{\mathrm{WT,Boi}}$, $P_m^{\mathrm{PV,Boi}}$ and $P_m^{\mathrm{BESS,Boi}}$ are the amount of electrical power that WT, PVs and BESS provide to the electric boiler for heating. $V_m^{\mathrm{Tank,CHP,E}}$, $V_m^{\mathrm{Tank,Fur}}$ and $V_m^{\mathrm{Tank,G}}$ are the amount of gas from the gas tank to the electrical generation of CHP, the furnace heating and the load supply, respectively. Summing the (A.6), (A.7) and (A.8), the following equation can be obtained.

$$P_m^{\mathrm{WT,E}} + P_m^{\mathrm{PV,E}} + P_m^{\mathrm{BESS,E}} = P_m^{\mathrm{WT}} + P_m^{\mathrm{PV}} + P_m^{\mathrm{BESS}} - Q_m^{\mathrm{Boi},1} / \eta^{\mathrm{Boi}} - V_m^{\mathrm{P2G},1} / \eta^{\mathrm{P2G}} \tag{A.11}$$

where $Q_m^{\mathrm{Boi},1} = P_m^{\mathrm{WT,Boi}}\eta^{\mathrm{Boi}} + P_m^{\mathrm{PV,Boi}}\eta^{\mathrm{Boi}} + P_m^{\mathrm{BESS,Boi}}\eta^{\mathrm{Boi}}$ and $V_m^{\mathrm{P2G},1} = P_m^{\mathrm{WT,P2G}}\eta^{\mathrm{P2G}} + P_m^{\mathrm{PV,P2G}}\eta^{\mathrm{P2G}} + P_m^{\mathrm{BESS,P2G}}\eta^{\mathrm{P2G}}$. Based on (A.10), the power balance of CHP can be derived, as follows,

$$P_m^{\mathrm{Tank,CHP,E,L}} = P_m^{\mathrm{Tank,CHP}} - P_m^{\mathrm{Tank,CHP,E,Boi}} - P_m^{\mathrm{Tank,CHP,E,P2G}} \tag{A.12}$$

By substituting (A.11) and (A.12) into the (A.3), (A.3) can be rewritten as (A.13).

$$L_m^{\mathrm{E}} = P_m^{\mathrm{WT}} + P_m^{\mathrm{PV}} + P_m^{\mathrm{BESS}} - Q_m^{\mathrm{Boi},1} / \eta^{\mathrm{Boi}} - V_m^{\mathrm{P2G},1} / \eta^{\mathrm{P2G}} + P_m^{\mathrm{Tank,CHP}} - Q_m^{\mathrm{Boi},2} / \eta^{\mathrm{Boi}} - V_m^{\mathrm{P2G},2} / \eta^{\mathrm{P2G}} \tag{A.13}$$

where $Q_m^{\mathrm{Boi},2} = P_m^{\mathrm{Tank,CHP,E,Boi}}\eta^{\mathrm{Boi}}$ and $V_m^{\mathrm{P2G},2} = P_m^{\mathrm{Tank,CHP,E,P2G}}\eta^{\mathrm{p2G}}$. Thus, (A.13) can be further reformulated as the linear and concise equation, as follows,

$$L_m^{\mathrm{E}} = P_m^{\mathrm{WT}} + P_m^{\mathrm{PV}} + P_m^{\mathrm{BESS}} - Q_m^{\mathrm{Boi}} / \eta^{\mathrm{Boi}} - V_m^{\mathrm{P2G}} / \eta^{\mathrm{P2G}} + P_m^{\mathrm{Tank,CHP}} \tag{A.14}$$

where $Q_m^{\mathrm{Boi}} = Q_m^{\mathrm{Boi},1} + Q_m^{\mathrm{Boi},2}$ and $V_m^{\mathrm{P2G}} = V_m^{\mathrm{P2G},1} + V_m^{\mathrm{P2G},2}$. Similarly, by substituting $Q_m^{\mathrm{Boi},1}$, $Q_m^{\mathrm{Boi},2}$, and $Q_m^{\mathrm{Fur}} = V_m^{\mathrm{Tank,Fur}}\eta^{\mathrm{Fur}}$ into (A.4), we can obtain

$$L_m^{\mathrm{H}} = Q_m^{\mathrm{Boi}} + Q_m^{\mathrm{Fur}} + P_m^{\mathrm{Tank,CHP}}\eta^{\mathrm{CHP,H}} / \eta^{\mathrm{CHP,E}} \tag{A.15}$$

Substituting (A.10) to (A.9), the amount of gas from the gas tank to gas load can be expressed as,

$$V_m^{\mathrm{Tank,G}} = V_m^{\mathrm{Tank}} - Q_m^{\mathrm{Fur}} / \eta^{\mathrm{Fur}} Q^{\mathrm{Gas}} - P_m^{\mathrm{Tank,CHP}} / \eta^{\mathrm{CHP,E}} Q^{\mathrm{Gas}} \tag{A.16}$$

Then, substituting $V_m^{\mathrm{P2G},1}$, $V_m^{\mathrm{P2G},2}$ and (A.16) into (A.5), Eq. (A.5) can be rewritten as,

$$L_m^{\mathrm{Gas}} = V_m^{\mathrm{P2G}} + V_m^{\mathrm{Tank}} - Q_m^{\mathrm{Fur}} / \eta^{\mathrm{Fur}} Q^{\mathrm{Gas}} - P_m^{\mathrm{Tank,CHP}} / \eta^{\mathrm{CHP}} Q^{\mathrm{Gas}} \tag{A.17}$$

Finally, Eq.(A.14), Eq.(A.15) and Eq.(A.17) can be written to the matrix form, as expressed in (7).

References

Aghdam, F.H., Kalantari, N.T., Mohammadi-Ivatloo, B., 2020. A stochastic optimal scheduling of multi-microgrid systems considering emissions: a chance constrained model. J. Clean Prod. 275, 122965.

Arefifar, S.A., Ordonez, M., Mohamed ,Y.A.I., 2017. Energy management in multi-microgrid systems—development and assessment. IEEE Trans. Power Syst. 32(2), 910-922.

Bui, V.H., Hussain, A., Im, Y.H., Kim, H.M., 2019. An internal trading strategy for optimal energy management of combined cooling, heat and power in building microgrids. Appl. Energy 239, 536-548.

Bui, V.H., Hussain, A., Kim, H.M., 2016. A multiagent-based hierarchical energy management strategy for multi-microgrids considering adjustable power and demand response. IEEE Trans. Smart Grid 9(2), 1323-1333.

Cui, H.T., Li, F.X., Hu, Q.R., Bai, L.Q., Fang, X., 2016. Day-ahead coordinated operation of utility-scale electricity and natural gas networks considering demand response based virtual power plants. Appl. Energy 176, 183-195.

Chicco, G., Mancarella, P., 2009. Matrix modelling of small-scale tri-generation systems and application to

operational optimization. Energy 34(3), 261-273.
Daneshvar, M., Mohammadi-Ivatloo, B., Asadi, S., Anvari-Moghaddam, A., Rasouli, M., Abapour, M., et al., 2020. Chance-constrained models for transactive energy management of interconnected microgrid clusters. J. Clean Prod. 271, 122177.
Dey, B., Bhattacharyya, B., Garcia Marquez, F.P., 2021. A hybrid optimization-based approach to solve environment constrained economic dispatch problem on microgrid system. J. Clean Prod. 307, 127196.
Deb, K., Jain, H., 2014. An evolutionary many-objective optimization algorithm using reference-point-based nondominated sorting approach, part I: solving problems with box constraints. IEEE Trans. Evol. Comput. 18(4), 577-601.
Deb, K., Pratap, A., Agarwal, S., Meyarivan, T., 2002. A fast and elitist multiobjective genetic algorithm: NSGA-II. IEEE Trans. Evol. Comput. 6(2), 182-197.
Dissanayake, A.M., Ekneligoda, N.C., 2020. Multiobjective optimization of droop-controlled distributed generators in DC microgrids. IEEE Trans. Ind. Inform. 16(4), 2423-2435.
Farina, M., Amato, P., 2004. A fuzzy definition of 'optimality' for many-criteria optimization problems. IEEE Trans. Syst. Man Cybern. A syst. Humans 34(3), 315-326.
Gansterer, M., Hartl, R.F., 2018. Collaborative vehicle routing: a survey. Eur. J. Oper. Res. 268(1), 1-12.
Hao, R., Ai, Q., Zhu, Y.C., Jiang, Z.Q., 2018. Decentralized self-discipline scheduling strategy for multi-microgrids based on virtual leader agents. Electr. Power Syst. Res. 164, 230-242.
Heitsch, H., Romisch, W., 2003, Scenario reduction algorithms in stochastic programming. Computat. Optimiz. Applicat. 24, 187–206.
Huang, Z.Y., Xie, Z.L., Zhang, C.Z., Chan, S.H., Milewski, J., Xie, Y., et al., 2019. Modeling and multi-objective optimization of a stand-alone PV-hydrogen-retired EV battery hybrid energy system. Energy Conv. Manag. 181, 80-92.
Jadhav, A.M., Patne, N.R., Guerrero, J.M., 2019. A novel approach to neighborhood fair energy trading in a distribution network of multiple microgrid clusters. IEEE Trans. Ind. Electron. 66(2), 1520-1531.
Jafari, A., Khalili, T., Ganjehlou, H.G., Bidram, A., 2020a. Optimal integration of renewable energy sources, diesel generators, and demand response program from pollution, financial, and reliability viewpoints: A multi-objective approach. J. Clean Prod. 247, 119100.
Jafari, A., Ganjehlou, H.G., Khalili, T., Bidram, A., 2020b. A fair electricity market strategy for energy management and reliability enhancement of islanded multi-microgrids. Appl. Energy 270, 115170.
Jiang, S.Y., Yang, S.X., 2016. An improved multiobjective optimization evolutionary algorithm based on decomposition for complex pareto fronts. IEEE T. Cybern. 46(2), 421-437.
Karimi, H., Jadid, S., 2020. Optimal energy management for multi-microgrid considering demand response programs: a stochastic multi-objective framework. Energy 195, 116992.
Khalili, T., Ganjehlou, H.G., Bidram, A., Nojavan, S., Asadi, S., 2021. Financial risk-based scheduling of micro grids accompanied by surveying the influence of the demand response program. In: 2021 IEEE/IAS 57th Industrial and Commercial Power Systems Technical Conference (I&CPS). IEEE, pp. 1-9.
Langer, L., Volling, T., 2020. An optimal home energy management system for modulating heat pumps and photovoltaic systems. Appl. Energy 278, 115661.
Liu, T.H., Zhang, D.D., Wang, S.Y., Wu, T., 2019. Standardized modelling and economic optimization of multi-carrier energy systems considering energy storage and demand response. Energy Conv. Manag. 182, 126-142.
Li, P., Li, R.X., Cao, Y., Li, D.Y., Xie, G., 2018. Multiobjective sizing optimization for island microgrids using a triangular aggregation model and the Levy-Harmony algorithm. IEEE Trans. Ind. Inform. 14(8), 3495-3505.
Lu, X.H., Zhou, K., Yang, S.L., Liu, H.Z., 2018. Multi-objective optimal load dispatch of microgrid with stochastic access of electric vehicles. J. Clean Prod. 195, 187-199.

Moeini-Aghtaie, M., Abbaspour, A., Fotuhi-Firuzabad, M., Hajipour, E., 2014. A decomposed solution to multiple-energy carriers optimal power flow. IEEE Trans. Power Syst. 29(2), 707-716.

Murty, V.V.S.N., Kumar, A., 2020. Multi-objective energy management in microgrids with hybrid energy sources and battery energy storage systems. Prot. Control Mod. Power Syst. 5(2), 1-20.

Shams, M.H., Shahabi, M., Kia, M., Heidari, A., Lotfi, M., Shafie-khah, M., et al., 2019. Optimal operation of electrical and thermal resources in microgrids with energy hubs considering uncertainties. Energy 187, 115949.

Shao, C.C., Wang, X.F., Shahidehpour, M., Wang, X.L., Wang, B.Y., 2017. An MILP-based optimal power flow in multicarrier energy systems. IEEE Trans. Sustain. Energy 8(1), 239-248.

Tan, B., Chen, H., 2020. Multi-objective energy management of multiple microgrids under random electric vehicle charging. Energy 208, 118360.

Wang, D.X., Qiu, J., Reedman, L., Meng, K., Lai, L.L., 2018. Two-stage energy management for networked microgrids with high renewable penetration. Appl. Energy 226, 39-48.

Wang, Y., Zhang, N., Kang, C.Q., Kirschen, D.S., Yang, J.W., Xia, Q., 2019. Standardized matrix modeling of multiple energy systems. IEEE Trans. Smart Grid 10(1), 257-270.

Wichmann, M.G., Johannes, C., Spengler, T.S., 2019. An extension of the general lot-sizing and scheduling problem (GLSP) with time-dependent energy prices. J. Bus. Econ. 89(5), 481-514.

Xu, D., Wu, Q.W., Zhou, B., Li, C.B., Bai, L., Huang, S., 2020. Distributed multi-energy operation of coupled electricity, heating and natural gas networks. IEEE Trans. Sustain. Energy 11(4), 2457-2469.

Xuan, A., Shen, X.W., Guo, Q.L., Sun, H.B., 2021. A conditional value-at-risk based planning model for integrated energy system with energy storage and renewables. Appl. Energy 294, 116971.

Yang, X.D., He, H.B., Zhang, Y.B., Chen, Y., Weng, G.Q., 2019. Interactive energy management for enhancing power balances in multi-microgrids. IEEE Trans. Smart Grid 10(6), 6055-6069.

Yang, Z., Hu, J.J., Ai, X., Wu, J.C., Yang, G.Y., 2021. Transactive energy supported economic operation for multi-energy complementary microgrids. IEEE Trans. Smart Grid 12(1), 4-17.

Yazdani-Damavandi, M., Neyestani, N., Shafie-khah, M., Contreras, J., Catalao, J.P.S., 2018. Strategic behavior of multi-energy players in electricity markets as aggregators of demand side resources using a bi-level approach. IEEE Trans. Power Syst. 33(1), 397-411.

Yuan, G.X., Gao, Y., Ye, B., Huang, R.P., 2020. Real-time pricing for smart grid with multi-energy microgrids and uncertain loads: a bilevel programming method. Int. J. Electr. Power Energy Syst. 123, 106206.

Zeng, B., Liu, Y., Xu, F.Q., Liu, Y.X., Sun, X.Y., Ye, X.M., 2021. Optimal demand response resource exploitation for efficient accommodation of renewable energy sources in multi-energy systems considering correlated uncertainties. J. Clean Prod. 288, 1-20.

Zhou, Q., Shahidehpour, M., Paaso, A., Bahramirad, S., Alabdulwahab, A., Abusorrah, A., 2020a. Distributed control and communication strategies in networked microgrids. IEEE Commun. Surv. Tutor. 22(4), 2586-2633.

Zhou, B., Zou, J.T., Chung, C.Y., Wang, H.Z., Liu, N., Voropai, N., et al., 2021. Multi-microgrid energy management systems: architecture, communication, and scheduling strategies. J. Mod. Power Syst. Clean Energy 9(3), 463-476.

Zhou, B., Cao, Y.P., Li, C.B., Wu, Q.W., Liu, N., Huang, S., et al., 2020b. Many-criteria optimality of coordinated demand response with heterogeneous households. Energy 207, 118267.

Zhang, Q., Li, H., 2007. MOEA/D: A multiobjective evolutionary algorithm based on decomposition. IEEE Trans. Evol. Comput. 11(6), 712-731.

Zhang, Y., Zhao Y.X., 2012. Analysis of the third party inspection strategy under asymmetric quality cost information. In: 2012 International Conference on Systems and Informatics (ICSAI). IEEE, pp. 1281-1286.